NUREG/CR-5082
ANL-88-1

Reactor Analysis and Safety Division

Simulation Experiments on Two-Phase Natural Circulation in a Freon-113 Flow Visualization Loop

by Sang Yong Lee and Mamoru Ishii

Argonne National Laboratory, Argonne, Illinois 60439
operated by The University of Chicago
Prepared for the Office of Nuclear Regulatory Research
U. S. Nuclear Regulatory Commission under Interagency Agreement DOE 40-550-75

Available from

Superintendent of Documents
U. S. Government Printing Office
Post Office Box 37082
Washington, D.C. 20013-7982

and

National Technical Information Service
Springfield, VA 22161

NUREG/CR-5082
ANL-88-1
(Distribution
Codes: R2
and R4)

ARGONNE NATIONAL LABORATORY
9700 South Cass Avenue
Argonne, Illinois 60439

SIMULATION EXPERIMENTS ON TWO-PHASE NATURAL CIRCULATION IN A FREON-113 FLOW VISUALIZATION LOOP

by

Sang Yong Lee* and Mamoru Ishii

Reactor Analysis and Safety Division

Report Completed: December 1987

Report Issued: January 1988

Prepared for the Division of Accident Evaluation
Office of Nuclear Regulatory Research
U.S. Nuclear Regulatory Commission
Washington, D. C. 20555
under Interagency Agreement DOE 40-550-75

NRC FIN No. A2026

---

*Department of Mechanical Engineering, Korea Advanced Institute of Science and Technology, Seoul, Korea.

SIMULATION EXPERIMENTS ON TWO-PHASE NATURAL CIRCULATION IN A FREON-113 FLOW VISUALIZATION LOOP

by

Sang Yong Lee and Mamoru Ishii

ABSTRACT

In order to study the two-phase natural circulation and flow termination during a small break loss of coolant accident in LWR, simulation experiments have been performed using a Freon-113 flow visualization loop. The main focus of the present experiment was placed on the two-phase flow behavior in the hot-leg U-bend typical of B&W LWR systems. The loop was built based on the two-phase flow scaling criteria developed under this program to find out the effect of fluid properties, phase changes and coupling between hydrodynamic and heat transfer phenomena. Significantly different flow behaviors have been observed due to the non-equilibrium phase change phenomena such as the flashing and condensation in the Freon loop in comparison with the previous adiabatic experiment. The phenomena created much more unstable hydrodynamic conditions which lead to cyclic or oscillatory flow behaviors. Also, the void distribution and primary loop flow rate were measured in detail in addition to the important key parameters, such as the power input, loop friction and the liquid level inside the simulated steam generator.

NRC FIN No.

A2026

Title

Phenomenological Modeling of Two-phase Flow in Water Reactor Safety Research

TABLE OF CONTENTS

LIST OF FIGURES

LIST OF TABLES

NOMENCLATURE

NOMENCLATURE

A	Non-dimensional area
a	Flow area
a_s	Solid cross sectional area
B	Biot number
C_p	Specific heat at constant pressure
d	Hydraulic diameter
F	Friction number
F_d	Pump characteristic number
f	Friction factor
g	Gravitational acceleration
h	Heat transfer coefficient
k	Thermal conductivity
K	Orifice coefficient
ℓ	Axial length
ℓ_h	Length of hot fluid section
L	Non-dimensional length
N_{pch}	Phase change number
N_{sub}	Subcooling number
N_{Fr}	Froude number
N_d	Drift flux number
N_f	Friction number (two-phase)
N_o	Orifice number
N_{th}	Thermal inertia ratio
$\dot{q}'''$	Heat generation density in solid
Q_s	Heat source number
R	Richardson number
St	Stanton number
t	Time
T	Temperature
T^*	Time ratio number
u	Velocity
V_{gj}	Drift velocity
x	Quality
x_e	Exit quality

Greek Symbols

α	Void fraction
α_e	Exit void fraction
α_s	Solid thermal diffusivity
β	Thermal expansion coefficient
δ	Conduction thickness
ΔH_{fg}	Latent heat of vaporization
ΔH_{sub}	Subcooling
Δp	Pressure drop
$\Delta\rho$	Density difference ($\equiv \rho_f - \rho_g$)
$\Delta\mu$	Viscosity difference ($\equiv \mu_f - \mu_g$)
μ	Viscosity
ξ	Wetted (heated) perimeter
ρ	Density

Subscripts

f	Liquid
g	Vapor
i	ith section
o	Reference constant (heated section)
R	Model to prototype ratio
s	Solid
$( )_m$	Model
$( )_p$	Prototype

EXECUTIVE SUMMARY

The main purpose of this study is to understand two-phase natural circulation phenomena in a hot-leg U-bend which is one of the important aspects of a small break loss of coolant accident in a Babcock and Wilcox (B&W) light water reactor. It is noted that in the prototype system, the diameter of the hot-leg is about 90 cm and the length to diameter ratio is relatively small at 20. This indicates that the two-phase flow in the hot-leg can be quite different from the standard small-scale experiments since the conventional two-phase models and correlations are developed based on the small diameter and large length to diameter ratio data. In view of this, the two-phase flow in a hot-leg has been studied in detail through experiments. A Freon-113 flow visualization loop for simulating the hot-leg U-bend natural circulation flow has been constructed based on the scaling criteria developed to find out the heat transfer and phase change effects. The experimental results showed that the flow behavior strongly depended on phase changes and coupling between hydrodynamic and heat transfer phenomena. They are summarized as follows:

- At the initial stage, the single phase natural circulation with a fairly long period is followed by cyclic flow behaviors. This cyclic flow behavior consists of stable two-phase flow, sudden flashing and suppression of boiling with flow termination. The cyclic flow behavior continues for three to six hours with a period of 4~15 minutes.
- The above unsteady flow is followed by a quasi-steady state with relatively stable flow. No large scale flow carry-over associated with violent flashing was observed. However, several regular patterns of flow oscillations are detected. These are the manometer oscillation with a period of 8~35 seconds and the density wave oscillation with a period of 2.5~4 minutes which is close to the residence time of a fluid around the loop.
- Along with a manometer oscillation, two different types of flow are observed. In the Type 1 oscillation, periodic mild flashing with a formation of short slug bubbles was observed with a sizable amount of flow carry-over through the inverted U-bend. In the Type 2 oscillation, a continuous slow boiling along the riser section of the hot-leg in bubbly flow mode induces small flow carry-over through the inverted

U-bend. Appearance of those types of oscillations depends strongly on the liquid level in the simulated steam generator as well as the power input and friction control valve openings.

- Significant variations of the void fraction were observed along the hot-leg. At the initial stage, the bottom section shows higher void fraction than the higher sections. This is due to the high-void churn-turbulent flow generated by 90° elbow at the bottom. However, near the top of the hot-leg, void fractions can become very high due to the large periodic flashing. At the later quasi-steady state mode, the void fraction increases along the hot-leg. This implies that, at the quasi-steady state, the boiling in the hot-leg is more important than the entrance effect of the 90° elbow.

- An average flow rate during the quasi-steady state mode depends on the liquid level inside the simulated steam generator. Especially, Type 1 oscillation induces relatively larger flow rates due to the formation of slug bubbles by mild flashing.

Through the present experiments, an understanding of the basic mechanism of the natural circulation and flow termination has been established. The power input, loop friction and the liquid level inside the simulated steam generator played key roles in determining natural circulation rate and flow behavior including flow oscillation inside the loop.

I. INTRODUCTION

Often, it is not practical to perform the full-scale testing for studying thermal-hydraulic phenomena in nuclear reactor system under abnormal operations or accident conditions due to safety reasons and high cost. The severity of the accident that occurred at Three Mile Island Unit-2 plant with its 2x4 loop NSSS design (Fig. 1) has increased interest in scaling of transient two-phase flow phenomena. In view of this, new scaling criteria for a two-phase system have been developed on a perturbation method applied to the system of governing equations by Ishii et al. [1,2]. These criteria have been used [3,4] to evaluate the design parameters of the new 2x4 simulation loop under the MIST program [5]. The extension of the criteria to the pressure scaling as well as the fluid to fluid scaling has also been studied in detail [6]. In view of certain scaling difficulties and scaling distortions in the integral facilities [5,7], a supporting experimental study to investigate the two-phase natural circulation, hot-leg U-bend two-phase flow behavior and associated scaling problems has been carried out at Argonne National Laboratory.

The major issues considered under this program are:

(1) natural circulation interruption and resumption,

(2) hot-leg two-phase flow regimes and regime transition,

(3) void distribution and relative velocity between phases,

(4) flow instability phenomena which may trigger loop-to-loop oscillations,

(5) any particular thermal non-equilibrium phenomenon which is important for natural circulation

(6) overall scaling effects in terms of geometries, pressure and fluid properties.

It is noted that in the prototype system, the diameter of the hot-leg is about 90 cm and the length to diameter ratio is relatively small at about 20. This indicates that the two-phase flow in the hot-leg can be quite different from the standard small scale experiments. There is a great uncertainty in describing the flow because the conventional two-phase flow

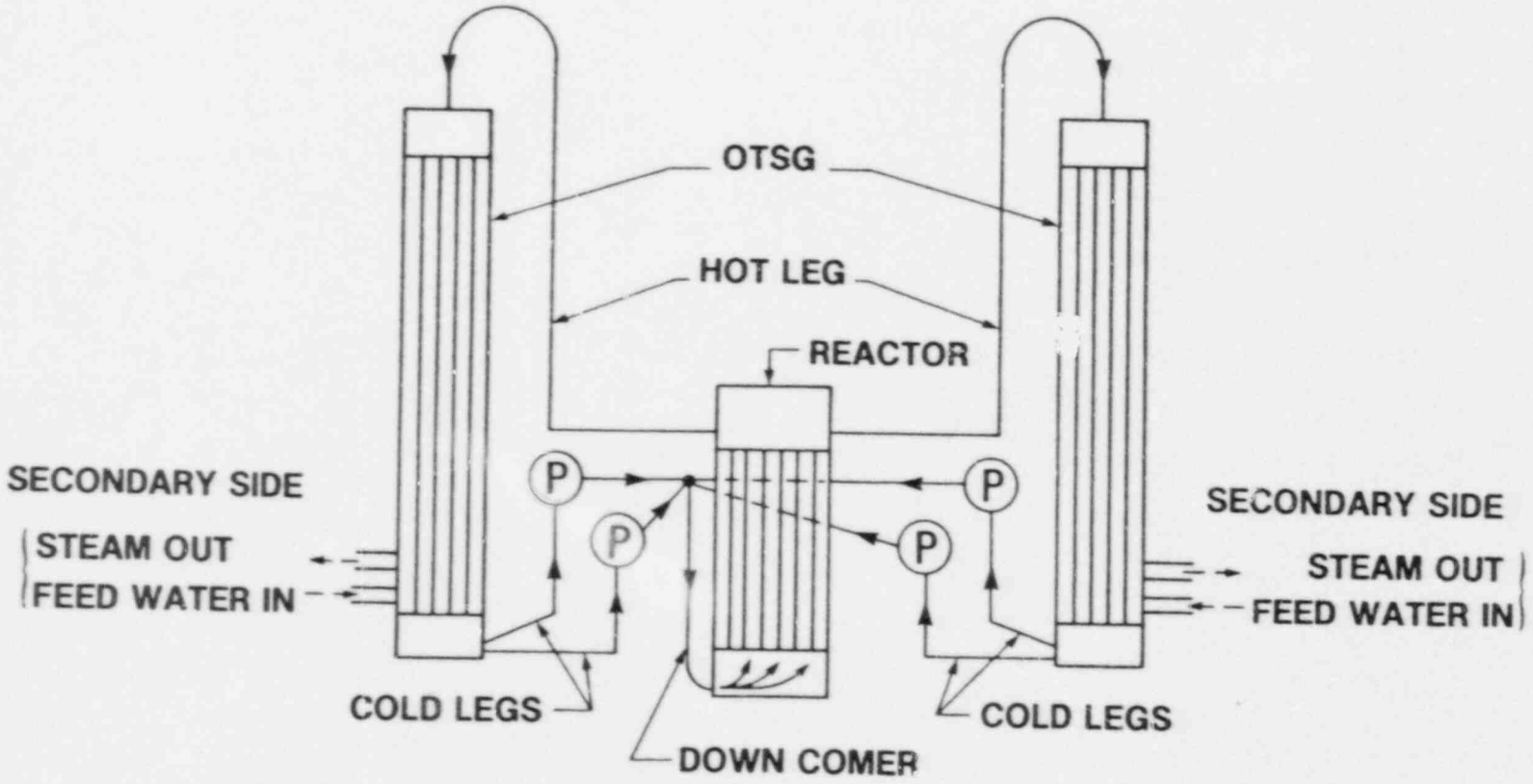

Fig. 1. Overall Schematic of 2 x 4 Loop Nuclear Reactor Model (Not to Scale)

models and correlations are developed based on small diameter and large length to diameter ratio system experiments. In view of this, the two-phase flow in a hot-leg has been studied in detail through experiments with an adiabatic flow visualization loop [8-10]. In present experiments, the effect of phase change and heat transfer by boiling and condensation was studied using the Freon-113 flow visualization loop.

II. BASIC SCALING CONSIDERATIONS

The available methods to develop similarity criteria for two-phase flow systems have been reviewed by Ishii and Jones [11]. The detail similarity analyses for a two-phase flow system have been carried out by Ishii and Zuber [12] and Zuber [13] among others. The results based on the local conservation equations and ones based on the perturbation method were utilized by Ishii and Kataoka [1] for developing scaling criteria for a thermal-hydraulic loop. The extension of the similarity analysis to a natural circulation system under both two-phase and single-phase condition was achieved by considering the scaling criteria from a small perturbation method. For this purpose, the relatively well-established drift-flux model and constitutive relations [14,15] were used. In the present study, the scaling criteria developed by Ishii and Kataoka [1] are applied.

The similarity parameters for the single-phase forced and natural circulation loop systems can be obtained from the integral effects of the local balance equations along the entire loop. A typical system consists of a thermal energy source, energy sink, connecting piping system between components, and a circulation pump. The dimensionless variables and parameters used in the similarity study are obtained from the dimensionless balance equations [1]. In these equations, the fluid properties are assumed to be constant except for the buoyancy term, where the Boussinesq approximation is used. The significant parameters are shown in Table I. Here, ΔT_o and u_o are the temperature difference and reference velocity which can be obtained by using the steady-state solution as follows:

$$\Delta T_o = \left(\frac{\dot{q}'''_o \ell_o}{\rho_f C_{pf} u_o}\right)\left(\frac{a_{so}}{a_o}\right) \tag{1}$$

Table I. Significant Dimensionless Similarity Parameters [1,3]

Single-phase Flow		Two-phase Flow	
Richardson No.:	$R \equiv g\beta\Delta T_o \ell_o / u_o^2$	Phase Change No.:	$N_{pch} \equiv \left(\frac{4\delta \dot{q}'''_o \ell_o}{d u_o \Delta H_{fg} \rho_f}\right)\left(\frac{\Delta\rho}{\rho_g}\right)$
Stanton No.:	$St \equiv 4h_i \ell_o / \rho_f C_{pf} u_o d_i$	Drift Flux No.:	$N_d \equiv V_{gj}/u_o$
Biot No.:	$Bi \equiv h_i \delta_{si}/k_{si}$	Density Ratio No.:	$N_\rho \equiv \rho_g/\rho_f$
Friction No.:	$F_i \equiv f_i\left(\frac{\ell_i}{d_i} + \frac{\ell_{ei}}{d_i}\right) + K_i$	Froude No.:	$N_{Fr} \equiv \frac{u_o^2}{g\ell_o \langle\alpha\rangle_o}\frac{\rho_f}{\Delta\rho}$
Pump Characteristic No.:	$F_d \equiv g\Delta H_d/u_o^2$	Friction No.:	$N_f \equiv \frac{f(\ell+\ell_e)}{d}\left(\frac{1 + X(\Delta\rho/\rho_g)}{[1+X(\Delta\mu/\mu_g)]^{1/4}}\right)\left(\frac{a_o}{a_i}\right)^2$
Time Ratio No.:	$T_i^* \equiv (\alpha_{si}/\delta_{si}^2)(\ell_o/u_o)$	Orifice No.:	$N_o \equiv K[1 + X^{3/2}(\Delta\rho/\rho_g)]\left(\frac{a_o}{a_i}\right)^2$
Heat Source No.:	$Q_{si} \equiv \frac{\dot{q}'''_{si}\ell_o}{\rho_{si} C_{psi} u_o \Delta T_o}$	Subcooling No.:	$N_{sub} \equiv \left(\frac{\Delta H_{sub}}{\Delta H_{fg}}\right)\left(\frac{\Delta\rho}{\rho_g}\right)$

Table I. Significant Dimensionless Similarity Parameters [1,3] (CONT'D)

Single-phase Flow	Two-phase Flow	
	CHF No.:	$N_q \equiv q'''_c/\delta\dot{q}'''_{so}$
	Time Ratio No.:	$T_i^* \equiv (\alpha_s \ell_o/u_o \delta^2)_i$
	Heat Source No.:	$Q_{si} \equiv \dfrac{\dot{q}'''_{si} \ell_o C_{pf}}{\rho_{si} C_{\mu si} u_o \Delta H_{sub}}$

$$u_o = \left[\frac{2\beta g (\dot{q}'''_o \ell_o / \rho_f C_{pf}) \ell_h (a_{so}/\ell_o)}{\sum_i (F_i/A_i^2)} \right]^{1/3} \tag{2}$$

where ℓ_o is the equivalent length.

In addition to the above defined physical similarity groups, several geometric similarity groups are defined:

Axial Length Scale: $L_i \equiv \ell_i/\ell_o$ (3)

Flow Area Scale: $A_i \equiv a_i/a_o$ (4)

It is noted here that the hydraulic diameter d_i of the ith section and the conduction depth δ_i are defined by

$$d_i \equiv 4\, a_i/\xi_i \tag{5}$$

and

$$\delta_i \equiv a_{si}/\xi_i \tag{6}$$

where a_i, a_{si}, ξ_i are the flow cross sectional area, solid structure cross sectional area, and wetted perimeter of ith section. Hence, d_i and δ_i are related by

$$d_i = 4(a/a_s)_i\, \delta_i \tag{7}$$

If the similarity is to be achieved between the natural circulation processes observed in the prototype and in the model, it should be

$$(A_i)_R = (L_i)_R = (\textstyle\sum F_i/A_i^2)_R = (R)_R = (St)_R = (T_i^*)_R = (Bi)_R = (Q_{si})_R = 1 \tag{8}$$

where subscript R denotes the ratio of the value of a model to that of the prototype, i.e.,

$$\Psi_R \equiv \frac{\Psi_m}{\Psi_p} = \frac{\Psi \text{ for model}}{\Psi \text{ for prototype}} \tag{9}$$

The frictional similarity requirement can be satisfied independently of the remaining scaling requirements. The overall friction similarity given by

$$\left(\sum_i F_i/A_i^2\right)_R = 1 \tag{10}$$

where

$$F_i = f_i\left(\frac{\ell_i}{d_i} + \frac{\ell_{ei}}{d_i}\right) + K_i \tag{11}$$

expresses that pipe friction loss and the minor losses associated with the loss coefficient can be interchanged without changing the overall value of the pressure loss term. By adding or removing bends or by providing additional flow restriction in the form of orifices, it should be possible to simulate a wide range of scaling conditions. However, for a scale-down system, some restrictions or limitations often exist [3].

As for the case of the single-phase natural circulation, similarity parameters for a closed loop system under a two-phase flow condition can be obtained from the integral effects of the local two-phase flow balance equations along the entire loop. Under a natural circulation condition, the majority of transients are expected to be relatively slow. Furthermore, for developing system similarity laws, the response of the whole mixture is important rather than the detailed responses of each phase and phase interactions. Therefore, the drift-flux model formulation is more appropriate for the derivation of system similarity parameters under a natural circulation condition. This is because the drift-flux model can properly describe the two-phase mixture-structure interactions over a wide range of flow conditions. The important dimensionless groups which characterize the kinematic, dynamic, and energetic similarity are given as Table I [1,3]. The Froude, friction and orifice number, together with the time ratio group, have their standard significance. The subcooling, phase-change and drift numbers are associated with the two phase flow system. The dimensionless groups shown in Table I must be equal in the prototype and model of the two-phase natural circulation flow, if the complete similarity requirements are to be satisfied. Thus,

$$(N_{pch})_R = (N_d)_R = (N_{Fr})_R = (N_f)_R = (N_o)_R = (N_{sub})_R = (T_i^*)_R$$

$$= (Q_{si}) = 1 \tag{12}$$

It can be shown from the steady-state energy balance over the heated section that N_{pch} and N_{sub} are related by

$$\left(\frac{\Delta\rho}{\rho_g}\right) x_e = N_{pch} - N_{sub} \tag{13}$$

where x_e is the vapor quality at the exit of the heated section. For a two-phase flow case, it is useful first to consider the effects of the proposed similarity criteria on the steam quality and void fraction. Under the phase change number and subcooling similarity, i.e., $(N_{pch})_R = (N_{sub})_R = 1$, Eq. (13) implies that

$$\left(x_e \frac{\Delta\rho}{\rho_g}\right)_R = 1 \tag{14}$$

This implies that the quality should be scaled by the density ratio, $\rho_g/\Delta\rho$. In addition to the above similarity, if the drift-flux number similarity $(N_d)_R = 1$ exists, then it can be shown that

$$\left(\alpha_e \frac{\Delta\rho}{\rho_f}\right)_R = 1 \tag{15}$$

This implies that the void fraction is scaled by the density ratio, $\rho_f/\Delta\rho$, which is near unity almost always. From this, the model void fraction should be very close to that of the prototype system. The results of the similarity law show the velocity ratio as

$$(u)_R = (\ell)_R^{1/2} \tag{16}$$

The time ratio is uniquely obtained as

$$(t)_R \equiv \left(\frac{\ell}{u}\right)_R = (\ell)_R^{1/2} \tag{17}$$

which implies that if the axial length is reduced in the model, then the real time simulation cannot be achieved in the two-phase natural circulation

loops. In such a case, the time events are accelerated (or shortened) in the scaled-down model by a factor of $(\ell)_R^{1/2}$ over the prototype.

A detailed model study for the plant design has been carried out and reported in Ref. [3]. The most severe condition in terms of the thermal-hydraulic simulation is imposed by friction number similarity, because in a scaled model the hydraulic diameter can be much smaller in piping system. Therefore, as mentioned earlier, for a given value for $(a)_R$, calculations are centered to determine $(\ell)_R$ to meet $(F_i)_R = 1$ for each section. The results from a series of calculations indicated that the hot-leg simulation imposes the strongest constraint [3]. Once the necessary condition for the hot-leg is obtained, the other sections are easily adjusted by increasing the minor loss coefficients. Thus, the basic scaling criterion from the hot-leg is presented. The prototype hot-leg flow resistance consists of the commercial steel pipe friction and the distributed loss due to elbows. The distributed loss factor, $(f_i \ell_{ei}/d_i)$, was calculated to be about 1.27 for the prototype. For a scaled model, lower $(f_i \ell_{ei}/d_i)$ value is desirable due to the friction number similarity requirement. Therefore, the friction factor for a drawn tubing is used. Furthermore, the practically minimum values for the flow restrictions are used.

Then, for single-phase and two-phase natural circulation system with time distortion, the maximum possible $(\ell)_R$ for given $(a)_R$ is given by [3]

$$(\ell)_R = 10.0 \left[1/(a)_R\right]^{-0.672} \tag{18}$$

and the volume ratio by

$$(V)_R = 10.0 \left[1/(a)_R\right]^{-1.672} \tag{19}$$

Hence, for a sample case of $(V)_R = 1/815$, one obtains for the practically optimum case as

$$(a)_R = 1/218$$
$$(\ell)_R = 0.27 \tag{20}$$

And in this case, the time scale is reduced by (Eq. (17)),

$$(t)_R = \frac{(t)_m}{(t)_p} = \sqrt{(\ell)_R} = 0.52 \qquad (21)$$

Therefore, the key timings of various transients will be reduced by a factor of 0.52 in the scale model. The prototype hot-leg diameter is 91.5 cm, vertical rise 14.25 m, and total length 21 m. By using these numbers, the corresponding model dimensions are 6.2 cm, 3.84 m and 5.6 m respectively. In view of the commercially available glass tubes, the diameters of 5 cm (2") and 10 cm (4") were chosen, and the vertical elevations of 3.5 m and 5.5 m were chosen to simulate the prototype flow as well as to study the scale distortion in the integral test facility, MIST. The cases of the adiabatic two-phase flow (Nitrogen-Water) experiments have been performed previously at Argonne National Laboratory [8-10]. In order to find out the effect of fluid properties and phase change, a separate Freon-113 loop with hot-leg diameter of 5 cm and length of about 6 m were constructed. The effect of the properties in scaling laws are summarized in Ref. [6]. The power of the heater section was determined by this scaling law for the case of decaying heat of 2% level of the full power, 4.1 MPa (600 psia) in prototype system with two hot-legs. About 1.5 KW of power turned out to be the proper value. The simulation of the two-phase flow in the integral test facility, MIST, by ANL facility is easier due to MIST's smaller flow area in comparison with the prototype. Basically, almost no restrictions such as Eq. (18) are necessary, since the hot-leg diameter of the present facility is 5 cm which is very close to that of MIST facility.

III. EXPERIMENTAL FACILITY

The overall loop schematic is shown in Fig. 2. This Freon-113 boiling and condensation loop was designed such that it could be operated either in a natural or in a forced circulation mode. The primary loop consists of the simulated core (heater section), hot-leg, U-bend, simulated steam generator (condenser), subcooler, loop friction control valve, expansion tank and pump. The loop pressure is regulated by the pressure at the free surface in the expansion tank. This pressure is maintained close to the atmospheric pressure by two pressure relief valves for the positive and negative

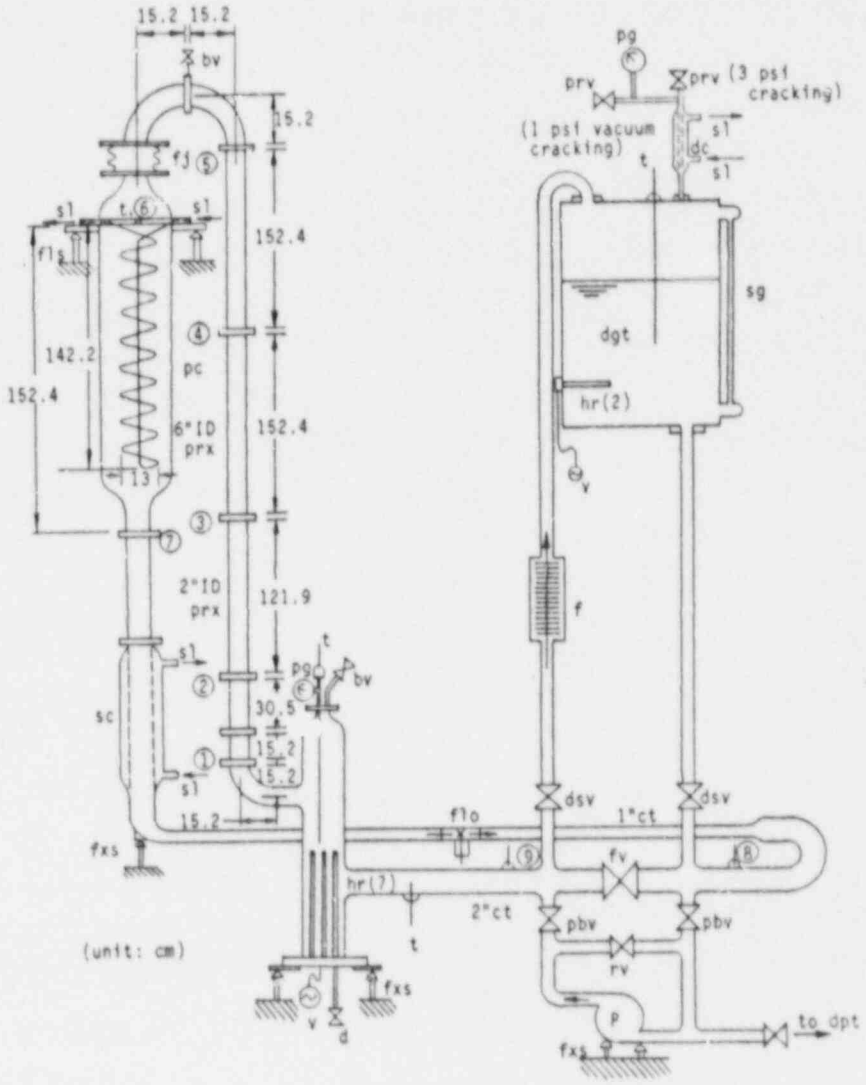

bv	bleed valve	P	pump (1.5 HP)
ct	copper tube (nominal size)	pbv	pump bypass valve
d	drain	pc	primary condenser (40 coil/ ¼" ct)
dc	dgt condenser (1" & 1¼" conc. ct)	pg	pressure gauge
dgt	degassing tank	prv	pressure relief valve
dpt	dump tank	prx	pyrex test section
dsv	degassing tank shut-off valve	rv	recirculate valve
f	filter	sc	subcooler (2" & 2½" conc. ct)
fj	flexible joint	sg	sight glass
flo	flowmeter	sl	flow to/from secondary loop
fls	flexible support	t	thermocouple
fxs	fixed support	v	variable transformer (0-4 KVA)
fv	friction control valve	①-⑨	pressure tap
hr	heating rod (7x600 W, 2x750 W)		

Fig. 2. Schematic of Freon-113 Flow Visualization Loop for Two-phase Natural Circulation Study

pressure cracking. Due to the hydrostatic head of the liquid Freon-113, the pressure at the simulated core is always above the atmospheric pressure, up to 159 KPa (23 psia). Basically, the two phase flow is generated by boiling of Freon-113 in the simulated core and condensed in the simulated steam generator which is cooled by the secondary loop. Freon-113 has a low saturation temperature of about 47°C at 1 atm. Thus the loop is operated at relatively low pressures and temperatures. The components and sections involving two-phase flow are designed to be transparent such that a flow visualization is possible. At present, the loop is approximately 6 m in height with the hot-leg inner diameter of 5 cm and the vertical elevation of about 5 m. The transparent sections were made of standard Corning Pyrex glass pipes and fittings. Other sections were made of copper tubes, brass fittings and stainless steel components.

The heat sink to the primary loop is supplied by the secondary Freon-113 loop (Fig. 3) consisting of the circulation pump, condenser coil (divided into upper and lower sections to change the cooling conditions), heat exchanger cooled by cold tap water and coils submerged in cold baths of antifreeze (ethylene-glycol) within a large chest-type freezer. The secondary loop is pressurized to 0.28 MPa above the atmospheric pressure (40 psig) and the coolant is always in the liquid state. Therefore, the thermal hydraulics of the secondary loop is not simulated in the present facility. The secondary side simply acts as a heat sink to the primary side in this design.

The simulated core is located at the bottom of the 5 cm (2") I.D. hot-leg. It was made of two Corning Pyrex tees of 10x5 cm size and a reducer of 10x5 cm. The volume of the actual core, core internal geometry and vessel downcomer were not simulated in the present design. The subcooled Freon-113 enters through the lower tee branch and exits through the upper tee branch stretched to the opposite direction (see Fig. 2). Seven electrical rods (immersion type heaters) of 0.95 cm O.D. and 30.4 cm length with the maximum power of 600 Watts per rod are used as a heat source. This corresponds to the total power capacity of 4.2 KW. The AC power is applied with two variac transformers for the control of the power input. The loop reference absolute pressure is measured by a Bourdon type pressure gauge connected to the top of the heater section. A sheathed thermocouple measures the temperature of fluid (Freon-113) inside the heater section.

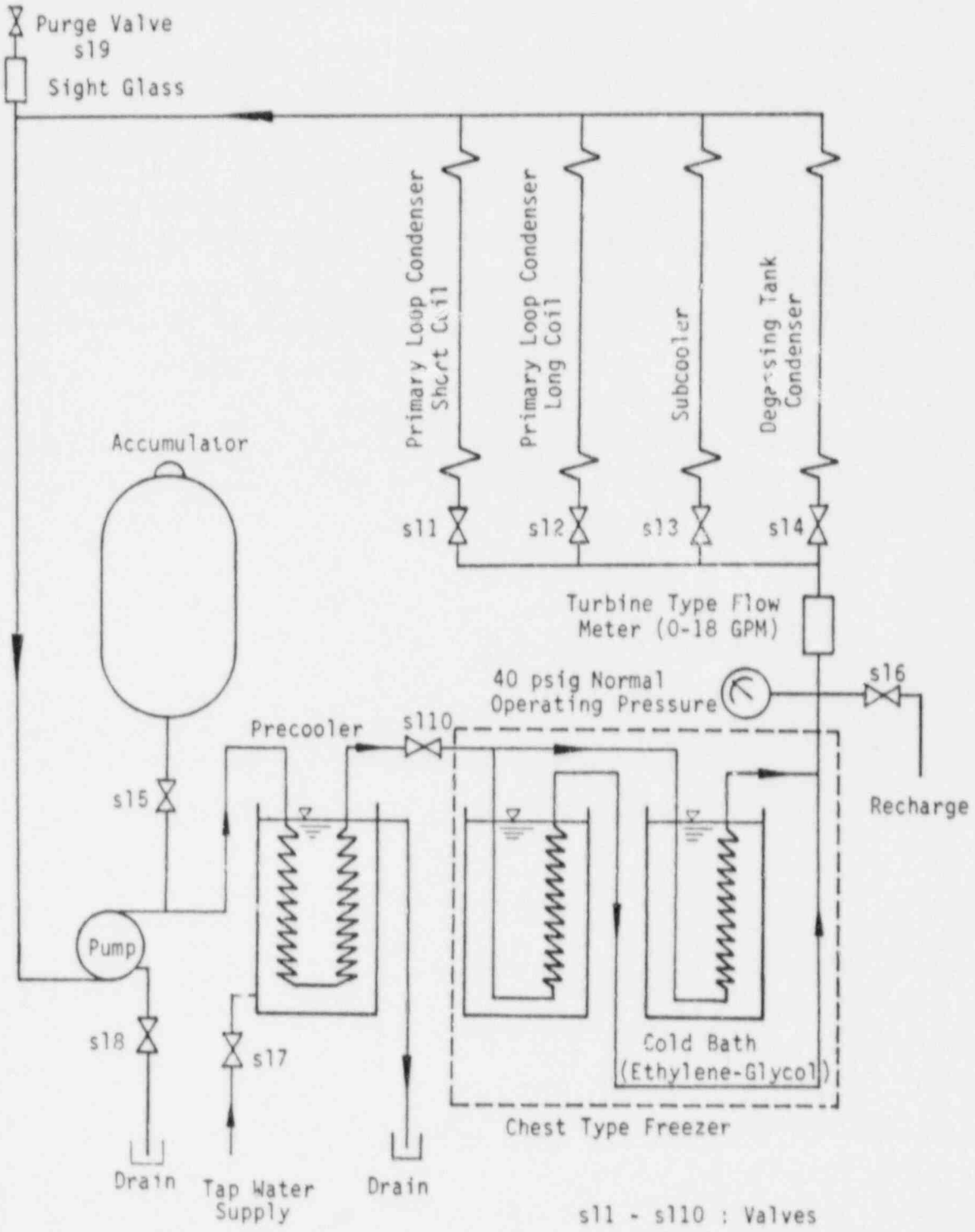

Fig. 3. Schematic of the Secondary Loop for Cooling

The riser section which corresponds to the hot-leg was made of Corning Pyrex glass pipes of 5 cm I.D. The total height of the hot-leg is 515 cm. The radius of the U-bend at the top of the loop is 15 cm. To measure the differential pressure, five pressure taps were installed along the hot-leg. The pressure tap plates of ring shape (5 cm I.D. and 8.9 cm O.D. with 1.3 cm thickness) was made of brass with a small hole of approximately 0.4 mm in diameter drilled in radial direction (i.e., perpendicular to the flow direction). Each plate was installed between glass pipes and sealed with Teflon gaskets (3.5 mm in thickness). The end of the pressure taps were connected to the SENSOTEC differential pressure transducers which were of strain gauge wet/wet type with low sensitivity to liquid temperature changes. These differential pressure transducers given accurate measurements of the void fractions in the hot-leg provided that the frictional pressure drop along the hot-leg is negligible relative to the gravitational head. The transducers have been selected in such a way that its range is as close to the operating range of each measuring point as possible to secure more accuracy in reading. The differential pressure transducers with the ranges of 0±13.8 KPa (0-±2 psi) and 0-±34.5 KPa (0-±5 psi) are used at the hot-leg section, see Table II.

Downstream of the hot-leg and U-bend, a bellows type flexible coupling of 5 cm length was used to absorb the thermal expansion and to reduce the stress at the glass test section. The steam generator is simulated by a simple coil condenser in a 15.2 cm I.D. and 152.4 cm long Pyrex glass pipe. The condenser was made of nominal 1/4" copper tube with 40 turns of 13 cm coil O.D. and 142.2 cm coil length. The condenser is divided into lower and upper sections to use either the entire coil or the upper half of the coil for condensation by simple valve operations. The primary coolant flows outside the condenser tube. The secondary loop Freon-113 fluid flows inside the tube and cools the primary fluid. Two pressure taps were installed at inlet and outlet of the primary side of the simulated steam generator to measure the void fraction (i.e., liquid level). The end of the pressure taps were also connected to the SENSOTEC differential pressure transducers of strain gauge wet/wet type with the range of 0-±68.9 KPa (0-±10 psi). Below the simulated steam generator, there is a Pyrex glass pipe of 5 cm I.D. and 152.4 cm length. Downstream of the pipe, there is a subcooler made of concentric copper tubes of 6.4 cm (2.5") and 5 cm (2") I.D., respectively. The effective length of

Table II. Channel Specification for the Data Acquisition System

Labtech Channel Number	Input Type	Location
17	Thermocouple 1 (Copper-Constantan)	Condenser coil inlet, upper coil cooling only
18	Thermocouple 2 (Copper-Constantan)	Condenser coil inlet, upper and lower coil
19	Thermocouple 3 (Copper-Constantan)	Condenser coil outlet
20	Thermocouple 4 (Copper-Constantan)	Degassing (expansion) tank
21	Thermocouple 5 (Copper-Constantan)	Heater section (simulated core)
22	Thermocouple 6 (Copper-Constantan)	Heater section inlet
23	Thermocouple 7 (Copper-Constantan)	Condenser (primary side)
33	Pressure Transducer (±2 psid max.)	1-2 (18" riser section)
34	Pressure Transducer (±5 psid max.)	2-3 (48" riser section)
35	Pressure Transducer (±5 psid max.)	3-4 (60" riser section)
36	Pressure Transducer (±5 psid max.)	4-5 (60" riser section)
37	Pressure Transducer (±10 psid max.)	6-7 (liquid level inside the condenser)
38	Pressure Transducer (±20 psid max.)	8-9 (pressure drop across the friction control valve)
5	Flow Rate (0-18 gpm)	Secondary loop*
6	Flow Rate (0-30 gpm)	Primary Loop

*Measures the total flow rate through the secondary loop pump.

the subcooler is 117 cm. This subcooler is also connected to the secondary loop for cooling, see Fig. 2.

The horizontal section of the loop was made of 2.5 cm (1") and 5 cm (2") nominal I.D. copper tubes connected in series as shown in Fig. 1. The above mentioned subcooler is followed by a 2.5 cm (1") I.D. section. A paddle wheel type turbine flow meter (SIGNET, MK515-P0) was installed to measure the liquid circulation rate of the primary side at the 1" I.D. section. The liquid flow rate can be read either from the panel indicator (SIGNET, MK584) or from the data acquisition system with microcomputer (IBM-PC/XT). It covers 0~1.89 liter/sec (0~30 gpm) with an accuracy of ±1% of the full scale. This corresponds to a range of the hot-leg liquid volumetric flux from 0 to 96 cm/sec. This paddle wheel type turbine flow meter is designed to have very little pressure loss and the accuracy is increased by reducing the flow area to one-fourth of the hot-leg section. The flow meter is located in the middle of the horizontal section with sufficient entrance length. The 2.5 cm (1") I.D. section is followed by a 5 cm (2") I.D. copper tube section. This section has a friction control valve (2" full port ball valve) to change the overall loop frictional resistance. In parallel to this valve, the primary circulation pump with a bypass and the expansion tank are connected.

The expansion tank of approximately 7×10^4 cm^3 is located near the top of the loop and connected to the pump suction side (see Fig. 2). This tank acts as a pressure regulating device and absorbs the volume changes of the coolant due to boiling and condensation. It can be also used as a degassing tank to eliminate dissolved gases and moisture from the Freon-113 inside the primary loop. For this purpose, the immersion type electric heater was installed near the bottom of the tank. This heater is used to boil Freon-113 in the tank, whereas the condenser at the top of the tank condenses back the vapor of Freon-113. The air and moisture can be purged to the outside of the loop through the relief valve. The top of the expansion tank is connected to the discharge side of the primary pump. A filter is located in the line. By using the primary pump, the coolant can be circulated through this filter and the expansion tank to eliminate impurity from the primary coolant.

In parallel with the friction control valve, there is a primary pump of shut-off head of 31 m (102 ft) powered by a 1.5 HP motor. During the natural circulation mode, this pump is isolated by valves. At the lowest point of the

loop near the suction side of the pump, a supply line for Freon-113 is connected to a storage tank of 0.5 m^3 which can be pressurized to 1.03 MPa above the atmospheric pressure (150 psig). The frictional pressure drop or the pump head is measured by the wet/wet type differential pressure transducer (SENSOTEC) with the operation range of 0-±138 KPa (0-±20 psi).

The primary side fluid temperature is measured at various key locations such as the heater section, inlets of heater section and simulated steam generator, by the immersion type sheathed thermocouples (Type-T, Copper-Constantan). For the extra protection of the glass test section, there are several pressure relief valves which are connected to a large coolant dump tank. At the top of the U-bend and the heater section, bleed valves were installed for a quick elimination of accumulated noncondensable gases just before each test run.

The temperatures of the secondary loop Freon-113 at the two inlets (for upper section and lower section respectively) and the exit of the condenser coil are also measured by the immersion type sheathed thermocouples (Type-T, Copper-Constantan).

All the analog signals from the thermocouples, pressure transducers and turbine type flow meters are read through the DASH-8 A/D board with two EXP-16 multiplexer boards and a STA-08 screw termination accessory board into the IBM-PC/XT using LTN (Labtech Notebook) software.

IV. EXPERIMENTAL PROCEDURES

Experimental measurements were performed using the Freon-113 loop with experimental parameters chosen as Table III. The initial conditions of the experiments for the primary side were

1) the single phase liquid state throughout the loop,

2) no initial flow,

3) an uniform temperature throughout the loop,

4) no cooling in the condenser (simulated steam generator).

Table III. Experimental Conditions and Experimental Specification Numbers (EXP. #)

Experimental Conditions		Secondary Loop Cooling			
		High Cooling	Med. Cooling	Low Cooling	No Cooling
Friction Control Valve Full-open	Heater Power 1.3 KW	#22	# 2	#32	#11
	Heater Power 2.2 KW	#24	#17	#34	#13
Friction Control Valve 1/4-open	Heater Power 1.3 KW	#26	#19	#33	#14
	Heater Power 2.2 KW	#28	#18	#35	#16

At the start of an experiment, a predetermined constant power was supplied to the simulated core, then it was kept until to the end of the experiment. The secondary loop was kept in the shutdown mode with no cooling to the primary loop until the U-bend portion at the top of the loop is filled by a substantial amount of the vapor. Then the subcooled liquid flow was initiated in the secondary loop with constant flow rate to activate the heat sink to the primary side. In the present test runs, the lower condenser coil and liquid subcooler were not used by closing the corresponding valves.

V. EXPERIMENTAL RESULTS AND DISCUSSIONS

A. Global (Overall) Phenomena

As explained in the experimental procedure, the loop operation was started by heating the liquid Freon-113 in the heater section with no initial flow and secondary cooling. The secondary loop circulation pump was then turned on when the primary loop was sufficiently heated, i.e., when a substantial amount of the vapor was accumulated at the top of the loop. During the experiments, several different loop-wise phenomena were observed as shown in Figs. 4-7; the phenomena appeared to be complicated, and depend on the experimental conditions. Here the typical loop-wise phenomena are going to be explained with the corresponding figures.

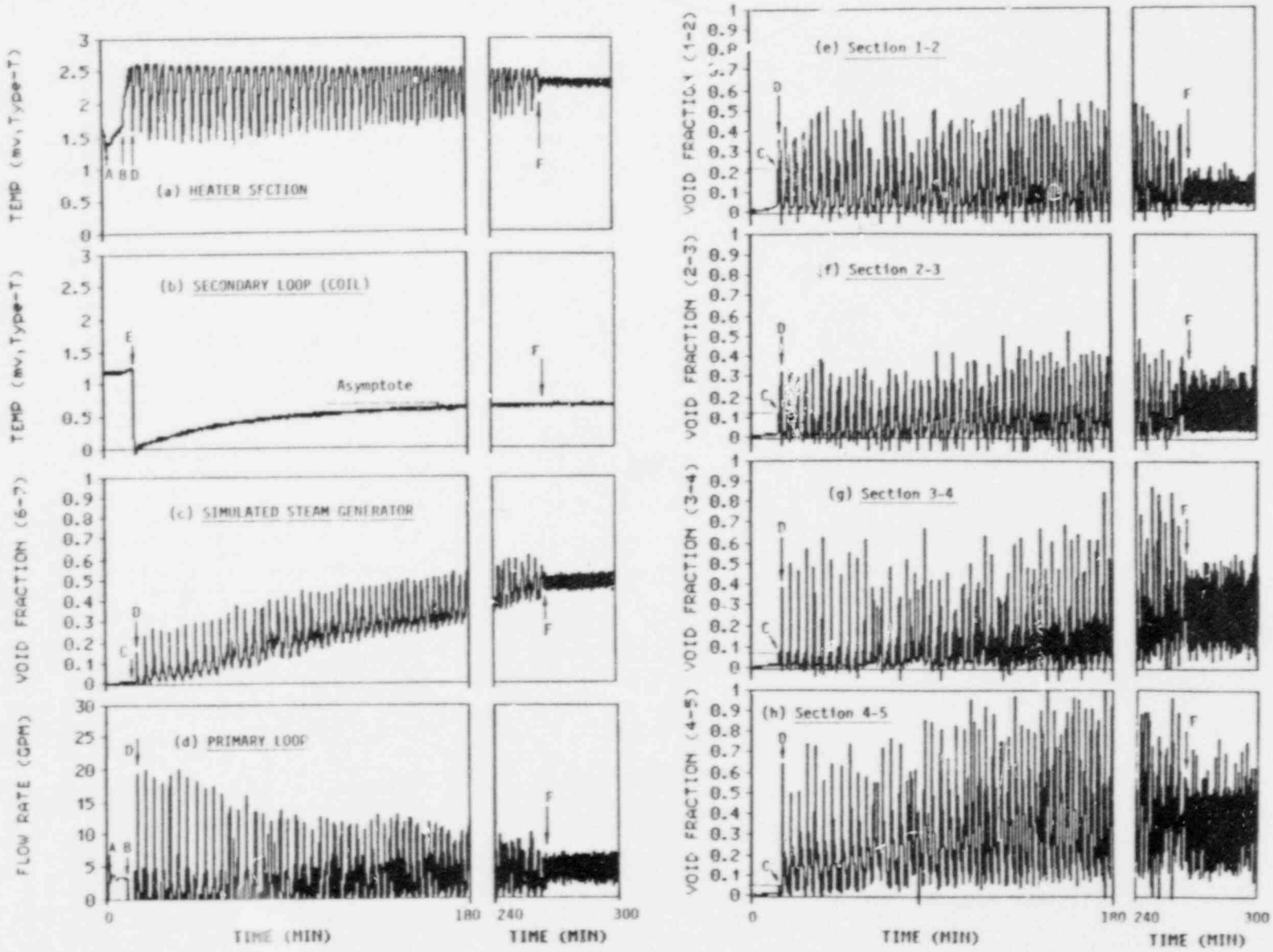

Fig. 4. Flow Behavior at Initial Stage (Friction Control Valve Full-open, Power Input 2.2 KW, High Cooling (Exp. #24))

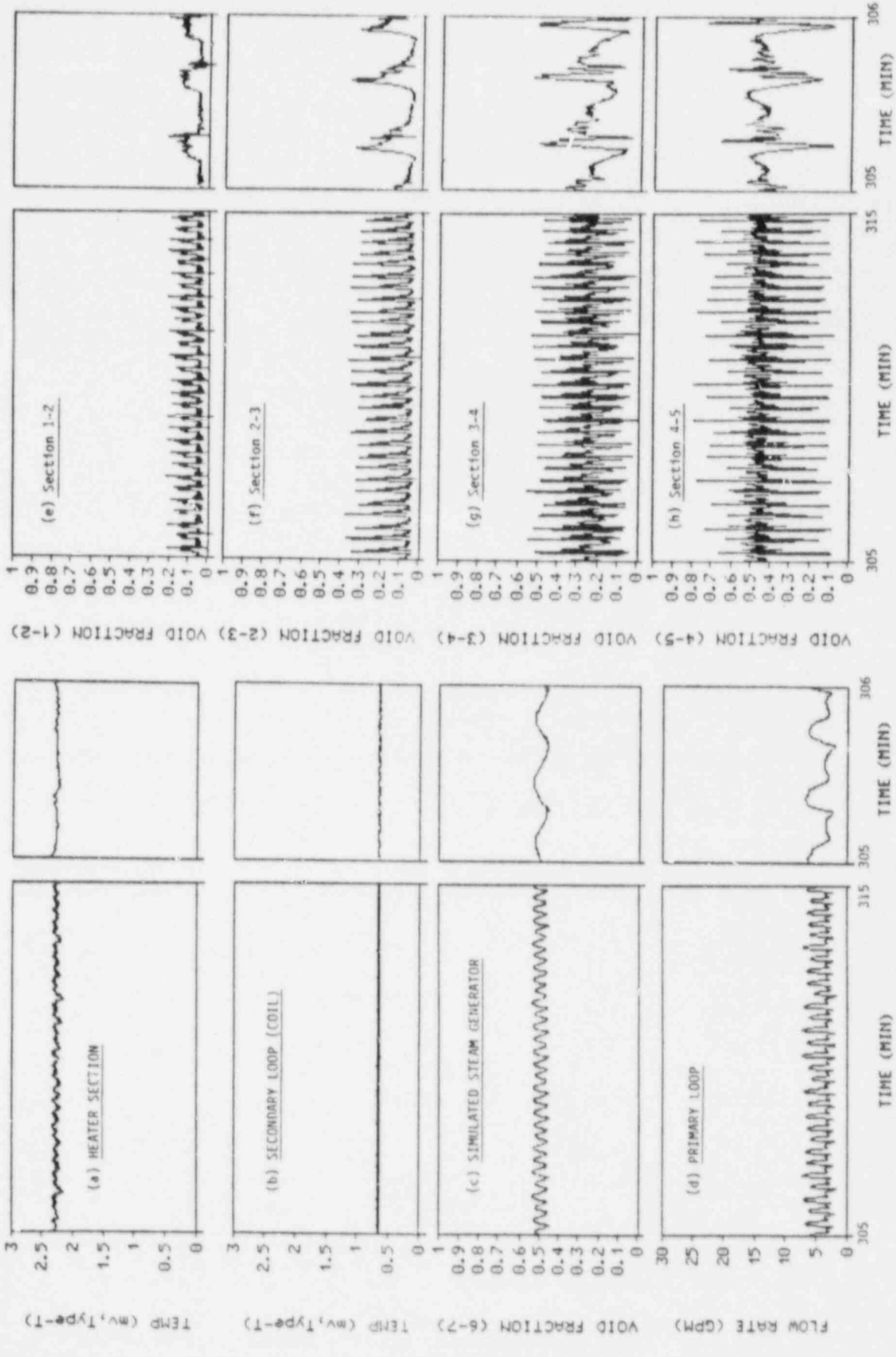

Fig. 5. Flow Behavior at Quasi-steady State (Type 1 Oscillation, Friction Control Valve Full-open. Power Input 2.2 KW, High Cooling (Exp. #24))

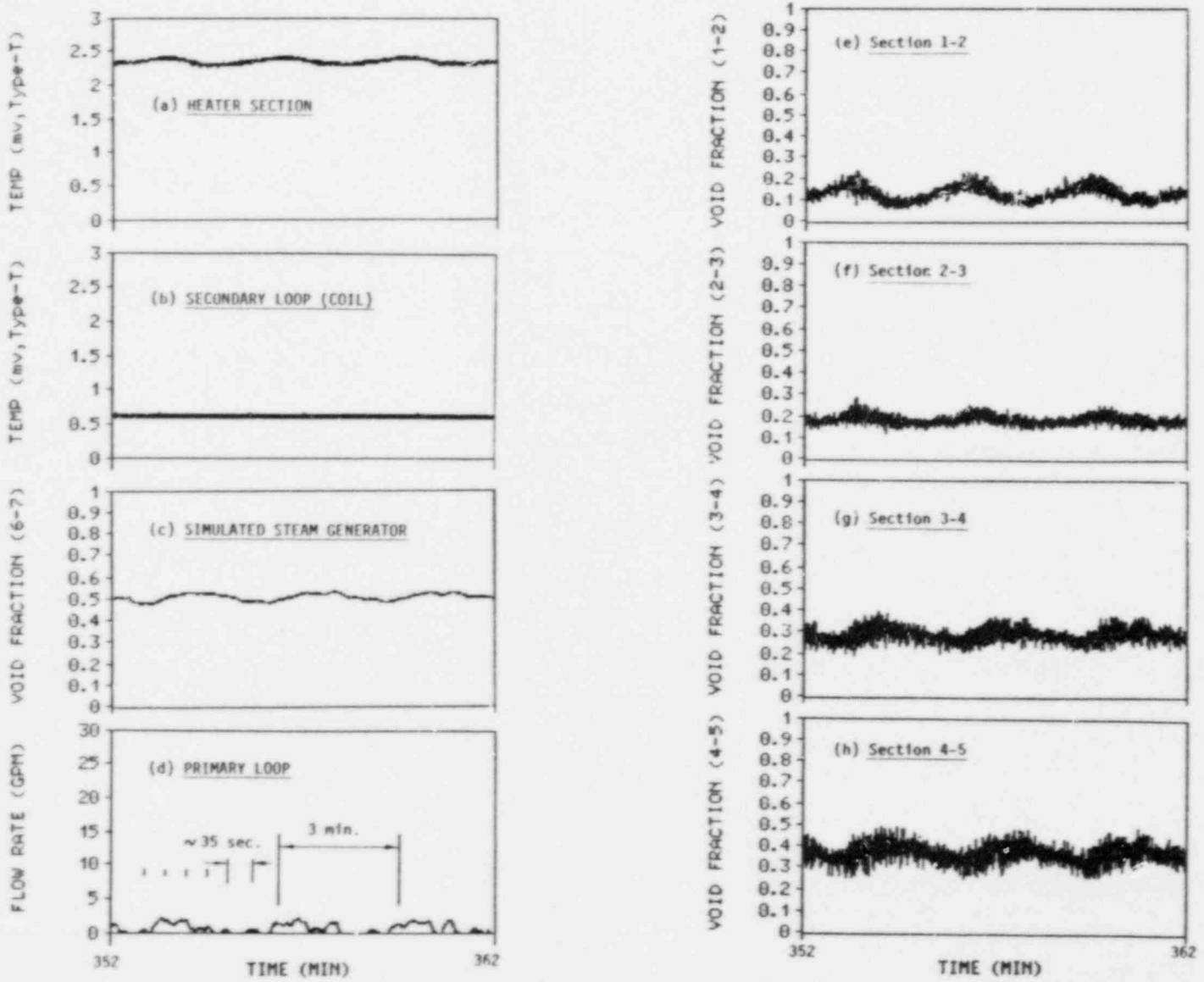

Fig. 6. Flow Behavior at Quasi-steady State (Type 2 Oscillation, Friction Control Valve 1/4-open, Power Input 2.2 KW, High Cooling (Exp. #28))

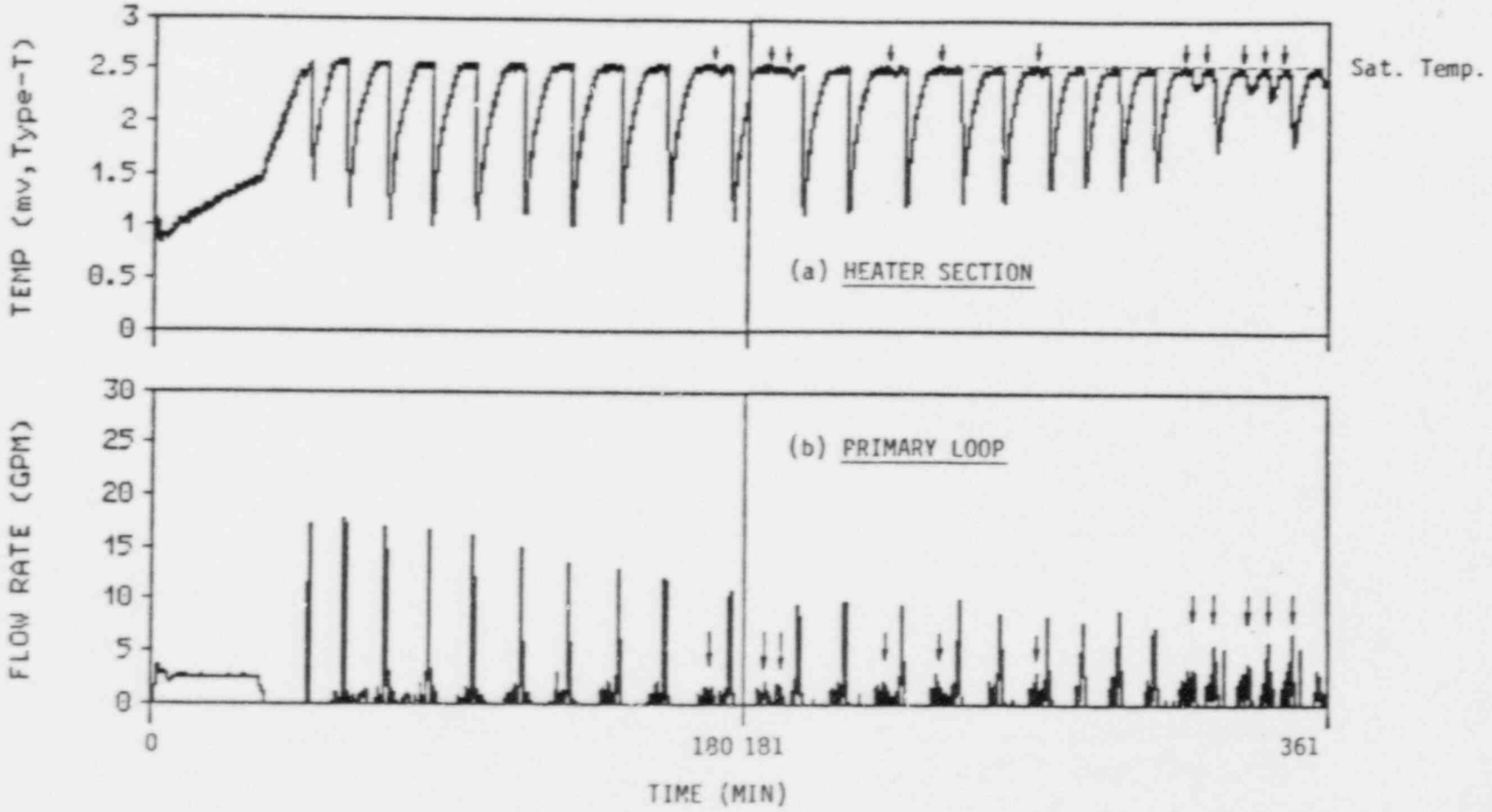

Fig. 7. Large Scale Flashing Triggered by the Density Wave Oscillation (Friction Control Valve Full-open, Power Input 1.3 KW, High Cooling (Exp. #22))

1. Initial Stage

At the beginning of the initial stage no loop-wise natural circulation of liquid was observed. The hot liquid column simply built up in the hot-leg by natural convections within the hot-leg. This state continues for a couple of minutes followed by the stable single (liquid) phase natural circulation over a fairly long period (7~39 minutes depending on the experimental conditions, Region A-B in Fig. 4(a) and 4(d)). The loop-wise natural circulation started when a sufficient head difference was established between the hot-leg (riser section) and the cold-leg (downcomer section) return. When the single phase natural circulation starts, the heater section temperature drops temporarily (Point A of Fig. 4(a)) and then increases gradually until the boiling starts in the simulated core (Point B of Fig. 4(a)). It was observed that the liquid flow rate was nearly constant (Region A-B in Fig. 4(d)). During this natural circulation, the vapor was slowly accumulated at the top of the loop which led to the termination of the single phase natural circulation.

The termination of the single phase natural circulation was followed by the boiling in the heater section, and the vapor started to accumulate at the space above the simulated core, which resulted in decrease of the liquid level inside the heater section. Once the liquid level reached the horizontal outlet of the heater section connected to the vertical rise of the hot-leg, the two-phase flow was established in the hot-leg, and eventually led to the two-phase natural circulation. Most of the vapor came from the vapor space above the simulated core. At the bottom of the vertical hot-leg, slugging occurred due to the flow stratification in the horizontal outlet of the heater section. However, the slug or cap bubbles immediately disintegrated into smaller bubbles. Initially, strong turbulent motions were observed and the bubble rise velocity was relatively small due to strong coupling between the liquid and vapor motion. Thus near the bottom of the vertical hot-leg, the void fraction appeared to be higher than the section above. (Compare the void fraction at Point C in Fig. 4(e) ~ Fig. 4(h).) Here the numbering of the axial sections corresponds to the pressure taps in the hot-leg section shown in Fig. 2. At this section, the flow regime was churn turbulent flow. Above this quite turbulent section, a typical bubbly flow was established up to the U-bend section. During this stage, a substantial amount of the vapor phase

accumulated at the U-bend section, which might lead to temporal flow terminations. The bubbly flow in the vertical hot-leg was maintained and the liquid level at condenser gradually came down. Figure 4(c) indicates the amount of vapor accumulated inside the condenser. At certain instances during this stage, occurrence of sudden flashing at the upper part of the hot-leg were observed. The main cause of this flashing appears to be the hydrostatic pressure decrease along the hot-leg which results in superheating of liquid and pressure fluctuations due to condensation in the simulated steam generator. Once the flashing started, the two-phase flow regime changed from bubbly to slug flow very rapidly, with the length of the slug bubble up to ~70 cm (Point D of Fig. 4(e) ~ Fig. 4(h)). Slug bubbles were generated by very rapid growth of nucleated bubbles in the hot-leg. Often, the bubble growth was so rapid that the liquid ahead of the slug bubble could not be accelerated sufficiently and the motion of the slug bubble slowed down considerably. Several cycles of the slug bubble generation led to a very much increased natural circulation rate (see Point D of Fig. 4(d)). Due to this increased flow rate, a considerable amount of subcooled liquid flowed into the heater section, and it resulted in complete suppression of the boiling (Point D of Fig. 4(a)); also the liquid level in simulated steam generator temporarily decreases considerably (Point D of Fig. 4(c)). This led to the termination of natural circulation. The stagnant liquid filled the lower part of the hot-leg and the heater section. The vapor filled the upper part of the hot-leg and U-bend section. The subcooled boiling started during this period and the whole process repeated within a period of 4-15 minutes depending on the boundary conditions imposed.

Cooling by the secondary loop can be started at any time during the experiment (Point E of Fig. 2(b)). The condensation of the accumulated vapor at the upper part of the condenser (simulated steam generator) results in reduction of the pressure in the hot-leg. This appears to promote the flashing phenomena.

2. Quasi-steady State

As cycles of the flashing continue (mostly for 3-6 hours), the whole flow phenomena may reach a certain quasi-steady state (Point F in Fig. 4(a)-(h)). The secondary loop coil temperature (Fig. 4(b) and Fig. 5(b))

reached a certain asymptote and the amplitudes of the fluctuation at the primary side became smaller. Once this state is reached, the flashing with large flow carry-over was not observed any longer. The bubbly flow, churn turbulent flow or small-scale slug flow maintained small intermittent flow carry-over through the inverted U-bend at the top of the loop. During this stage, the temperature of the fluid (Freon-113) in the heater section remained at almost constant due to the saturation condition (Fig. 4(a) or Fig. 5(a)). However, certain regular patterns of flow oscillation were observed (Figs. 5, 6). Here, they are named as Type 1 and Type 2 respectively. Along with those two different types of oscillations, two dominant ranges of oscillatory periods were detected; they are 8~35 sec. and 2.5~4 min. respectively. For example, in Fig. 5(c)~(h), an oscillation mode with a period of ~20 sec was clearly observed. Or, as in Fig. 6(a) and Fig. 6(c)~(h), Type 2 oscillation with two dominant frequencies (~35 sec. and ~3 min.) is observed.

At the beginning of each cycle of Type 1 oscillation, the liquid level in the heater section is slightly higher than the horizontal outlet of the heater section connected to the riser section of the hot-leg. Due to the regular oscillation of the liquid level with continuous boiling inside the heater section, the liquid level gradually approaches the horizontal outlet, and the vapor begins to flow into the riser section. The temperature of the fluid in the riser section remains almost in saturated condition corresponds to the hydrostatic pressure. Since the hydrostatic pressure decreases along the riser section, the fluid flowing into the hot-leg becomes slightly superheated as it rises up. Thus the vapor introduced into the riser section becomes a short slug bubble by rapid evaporation (see the sharp peaks in Fig. 5(e)~(h)) as it moves up, which induces sizable amount of flow rate. See the peaks of the flow rate in Fig. 5(d). This disturbs and changes the liquid levels inside the simulated steam generator and the heater section temporarily, and the whole process repeats with a cyclic period of ~20 sec. Unlike the initial stage, the temperature inside the heater section remains in saturated condition. This is due to the lower subcooling and smaller flow rate of incoming fluid than the initial stage. This oscillation with a period of ~20 sec. turned out to be a manometer oscillation.

In Type 2 oscillation, the liquid level in the heater section remains almost stationary with continuous flow of vapor into the riser section. The

flow carry-over is maintained by bubbly flow generated by continuous slow boiling; thus the void fraction becomes very steady with a longer period (2.5-4 min.) of oscillations (see Fig. 6(e)-(h)). Also, the liquid level inside the simulated steam generator (i.e., the condensing boundary) oscillates with the same cyclic period. This long-period signal comes from the density wave oscillation. Along with this longer period oscillation, a manometer oscillation having ~35 second-period is also observed as can be seen in Fig. 6(d).

Large flow carry-over with flashing (unsteady behavior) shown in the initial stage seems to be triggered by the density wave oscillations if the system is in unstable flow conditions. Figure 7 illustrates this behavior properly. Once the temperature of the fluid in the heater section reaches close to the saturation temperature (top flat portions of each cycle in Fig. 7(a)), density wave causes flow oscillations as indicated by arrows in Fig. 7, and triggers large flow carry-over. However, as the cycle continues, the overall loop temperature reaches a certain quasi-steady state, and the peak flow rate (Fig. 7(b)) and temperature fluctuation (Fig. 7(a)) by large flow carry-over decrease. This eventually leads the two types of oscillations indistinguishable, and then the density wave oscillation is detected only. For the case of Fig. 4, the periods of large flow carry-over and density wave oscillation are indistinguishable from the beginning since the time required for heating up of the liquid in the heater section to the saturation temperature is shorter than the case of Fig. 7 due to higher power input.

B. Analysis of Experimental Data

1. Initial Stage

a. Single-phase Natural Circulation and Flashing

As mentioned earlier, at the beginning of the initial stage, the single phase natural circulation was observed. Tables IV and V and Fig. 8 show the effects of the power input and friction control valve openings on the single phase natural circulation. The durations and flow rates shown in Table IV are the averaged value of several trials for each experimental conditions. The single phase natural circulation flow rate increases as the power input and the opening of the friction control valve increases. However, the duration of the single phase circulation decreases as the power input increases.

Table IV. Single Phase Natural Circulation

Friction Control Valve / Power Input (KW)	Full-open		1/4-open	
	Duration (min.)	Flow Rate (gpm)	Duration (min.)	Flow Rate (gpm)
1.3	26.5	2.5	23.0	1.1
2.2	12.1	3.4	10.3	1.4

Table V. Cyclic Period of Flashing/Large Flow Carry-over
(unit: min)

Friction Control Valve Opening	Power (Heat) Input (KW)	Secondary Cooling Rate		
		High Cooling	Med. Cooling	Low Cooling
Full-Open	1.3	14.0	13.0	15.2
	2.2	4.0	3.8	3.7
1/4-Open	1.3	11.5	10.6	12.2
	2.2	4.2	4.5	4.1

The overall temperature rises rapidly in case of higher power input which leads to the earlier incipience of boiling phenomena. The effect of the opening of the friction control valve on the duration of this single phase flow seems to be minor. However, if the loop friction increases, the flow rate decreases. This results in build-up of higher temperature locally at the heater section and eventually the boiling starts somewhat earlier.

After the termination of single phase natural circulation, the subcooled and saturated boiling occurred and then flashing with large flow carry-over followed. The whole process repeated with certain period. The period of this cyclic behavior also depends on the experimental conditions (Table V).

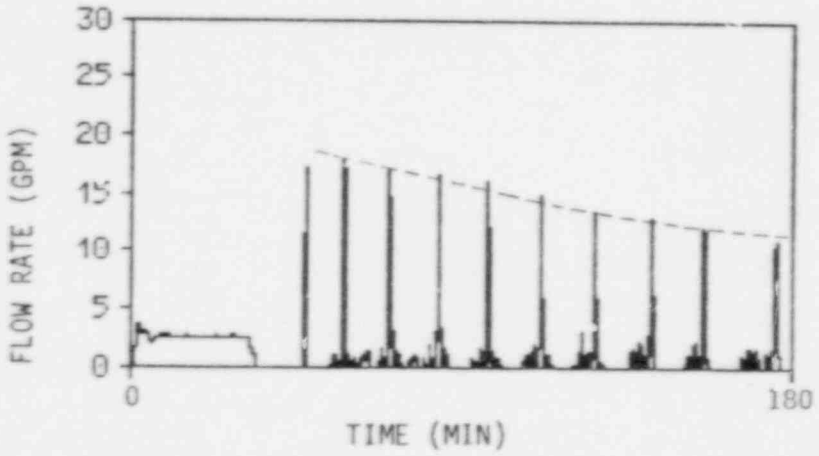

(a) Friction Control Valve Full-open, Power Input 1.3 KW

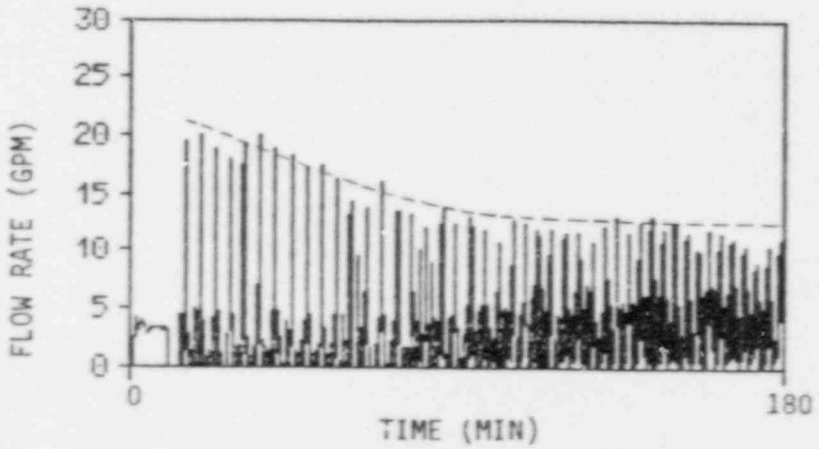

(b) Friction Control Valve Full-open, Power Input 2.2 KW

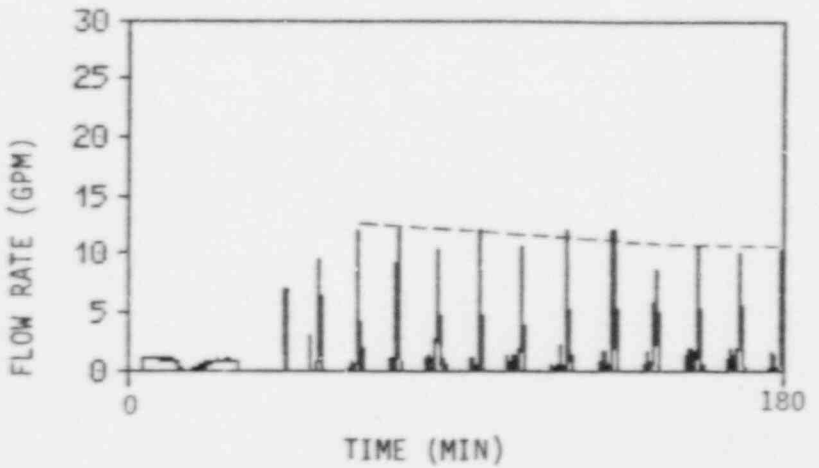

(c) Friction Control Valve 1/4-open, Power Input 1.3 KW

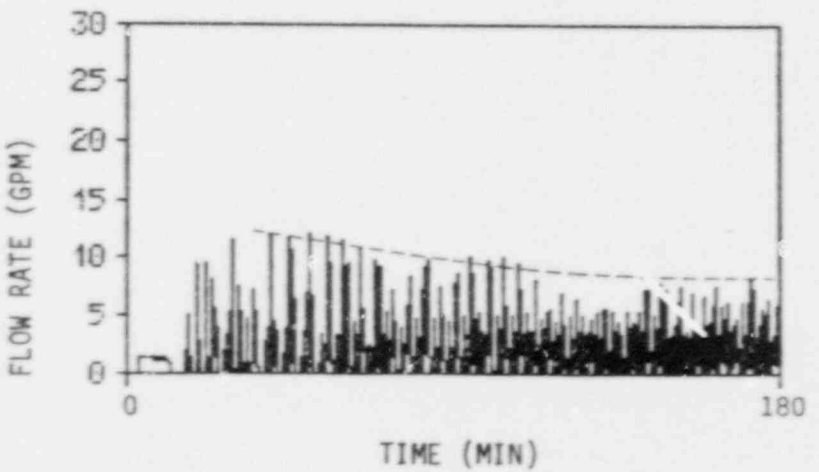

(d) Friction Control Valve 1/4-open, Power Input 2.2 KW

Fig. 8. Primary Loop Flow Rate at Initial Stage (0-180 min.), High Cooling

Little difference is observed between the periods with different cooling rates. However, the effect of the power input was significant. The period of this cyclic behavior decreases considerably with the increase of power input. That can be explained as follows. The flashing and large flow carry-over occur when the two phase bubble column is fully established in the hot-leg portion with its density low enough (compared with the liquid density in the cold-leg portion) to induce the two-phase natural circulation. Also, the maximum flow rate depends on the density difference between bubble column inside the hot-leg and liquid column in the cold-leg. Once the pressure of the system is fixed to a certain value, the density difference required for the flashing with large flow carry-over tends to be constant regardless of power input. The peak flow rates appear to be about the same as in Fig. 8(a) and (b). However, the time required for heating up to the saturated condition depends on the power input significantly. The period of flashing becomes shorter with higher power input. The effect of the valve opening on the period of flashing seems to be relatively minor. At low power input, as shown in Table V and Fig. 8(a) and (c), the peak flow rate appears to be smaller with smaller friction control valve-opening. Then from the overall energy balance, it can be said that the flashing should occur more frequently in order to transfer the same amount of heat from the heater section to the condenser by natural circulation. On the other hand, in case of high power input (Table V and Fig. 8(b) and (d)), the primary flow rate depends mostly on the small-scale flow carry-over, and the decrease of peak flow rate by reducing the friction control valve-opening does not affect much on the period of flashing.

b. Void Fraction

Figure 9 shows the peak and average values of void fractions of each riser section along the hot-leg (see Fig. 2 for the location of each riser section). In case of the friction control valve full-open (Fig. 9(a) and (c)), the bottom section (1-2) data shows higher time average void fraction than those at the next two sections (2-3 and 3-4). This can be explained as follows. The 90° elbow at the bottom of the vertical hot-leg generate large eddies and vortices. Due to the strong secondary flow effect, disintegrated bubbles are moving in the mode of the churn turbulent flow which leads to reduced relative velocity and higher void fraction. This effect dies

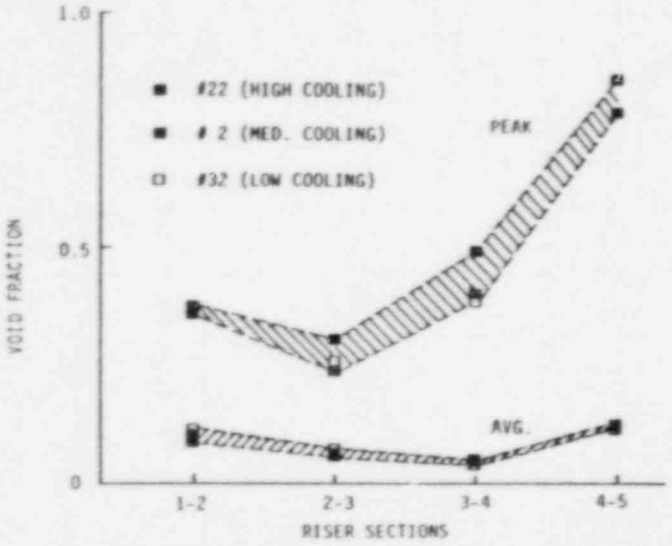

(a) Friction Control Valve Full-open, Power Input: 1.3 KW

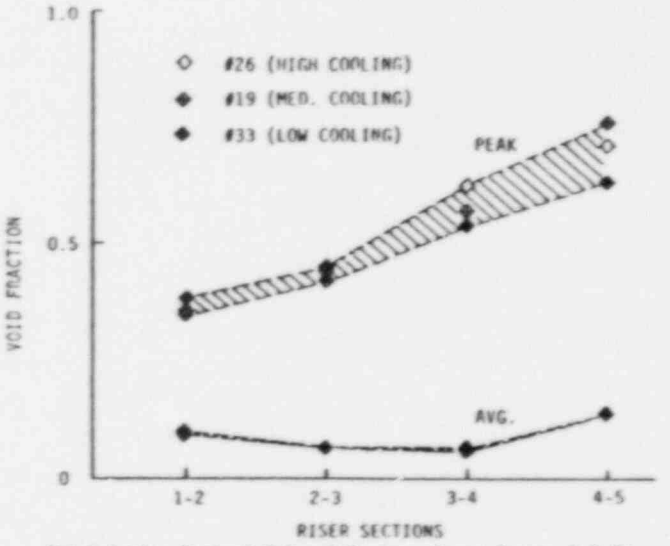

(b) Friction Control Valve 1/4-open, Power Input: 1.3 KW

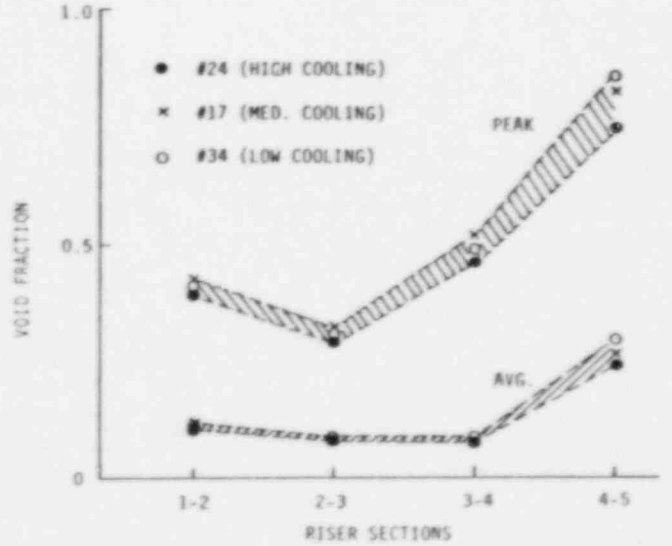

(c) Friction Control Valve Full-open, Power Input: 2.2 KW

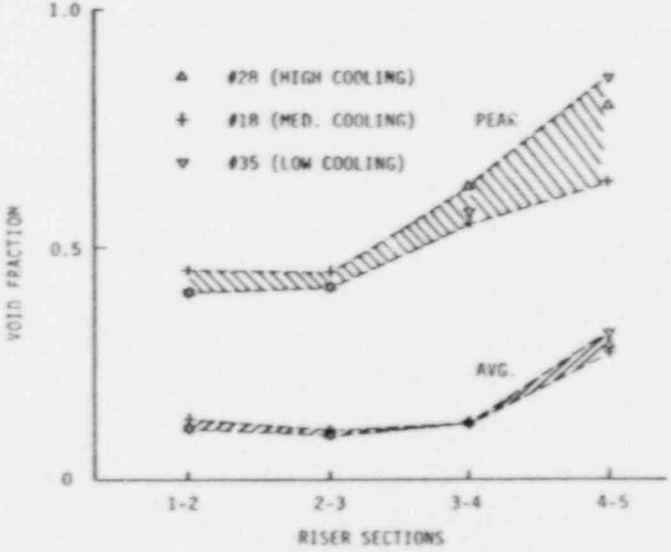

(d) Friction Control Valve 1/4-open, Power Input: 2.2 KW

Fig. 9. Void Fractions of Eacn Riser Section of Hot-leg (Initial Stage, 60-90 min.)

rapidly as bubbles move upward as indicated by the lower void fractions in the next two sections. However, in section 3-4, occurrence of slug bubbles with flashing cause much higher peak void fractions. This behavior is more pronounced at the top section (4-5) which has the highest peak void fraction. The highest average void fraction is detected also at this section (see also Fig. 4(e)-(h) and Fig. 10(a)-(d)).

Similar behavior was observed in case of friction control valve 1/4-open. However, the peak void fraction monotonously increases along the riser section (see Fig. 9(b) and (d) and Fig. 11(a) and (b)), since slug bubbles start to grow at the lower section of the hot leg. This seems to be due to the longer residence time of fluid passing through the heater section, and the fluid temperature at the lower part of the hot-leg becomes high enough to start flashing in comparison with the case of friction control valve full-open.

2. Quasi-steady State

Averaged values of experimental data at quasi-steady state are listed in Table A-1 in the Appendix with the corresponding channel numbers and the experimental specification numbers shown in Table II and Table III respectively.

a. Void Fraction

Figure 12 shows the void fractions of each riser section at quasi-steady state with various experimental conditions. All the plots in Fig. 12 shows the trend that the void fraction increases as the fluid climbs up the riser section of the hot-leg. This is caused by the decrease in the saturation temperature corresponding to the hydrostatic pressure at each riser section. For the case of the high power input with the friction control valve full-open (Fig. 12(a)), sudden changes in the hot-leg void fractions at a certain liquid level of the simulated steam generator (condenser) are observed. That is, as the liquid level of the simulated steam generator decreases, the flow behavior changes from one type (Type 1) to another (Type 2). In this case the void fractions of the first three sections from the bottom (1-2, 2-3, 3-4) increase whereas the void fraction at the top section (4-5) decreases. This is because, as explained earlier, slug bubbles form inside the hot-leg in Type 1 flow. This leads to higher-void flow at the top section. If the opening of the friction control valve decreases (Fig. 12(b)),

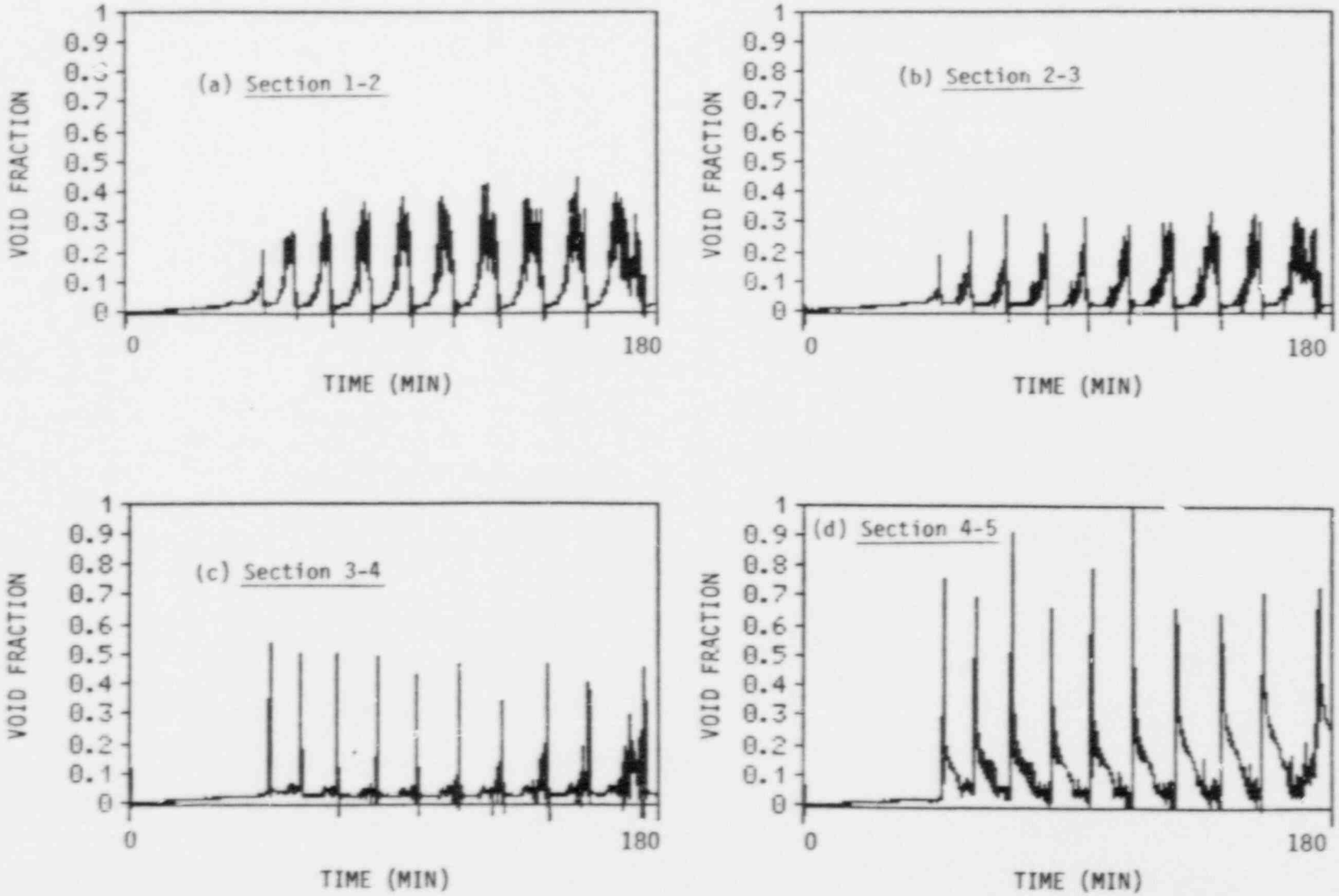

Fig. 10. Void Fraction of Each Riser Section of Hot-leg (Initial Stage, Friction Control Valve Full-open, Power Input 1.3 KW (Exp.#22))

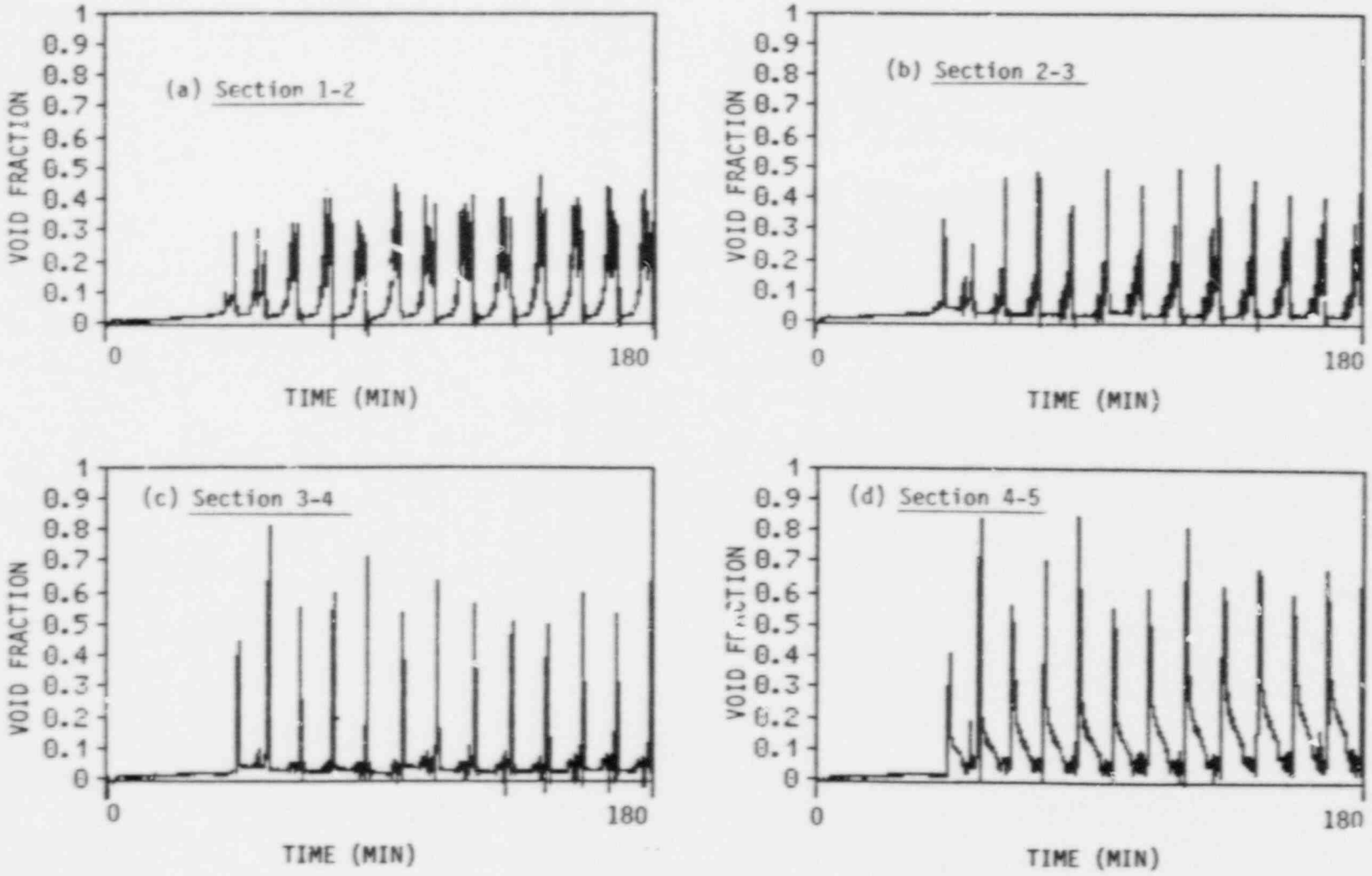

Fig. 11. Void Fraction of Each Riser Section of Hot-leg (Initial Stage, Friction Control Valve 1/4-open, Power Input 1.3 KW (Exp.#26))

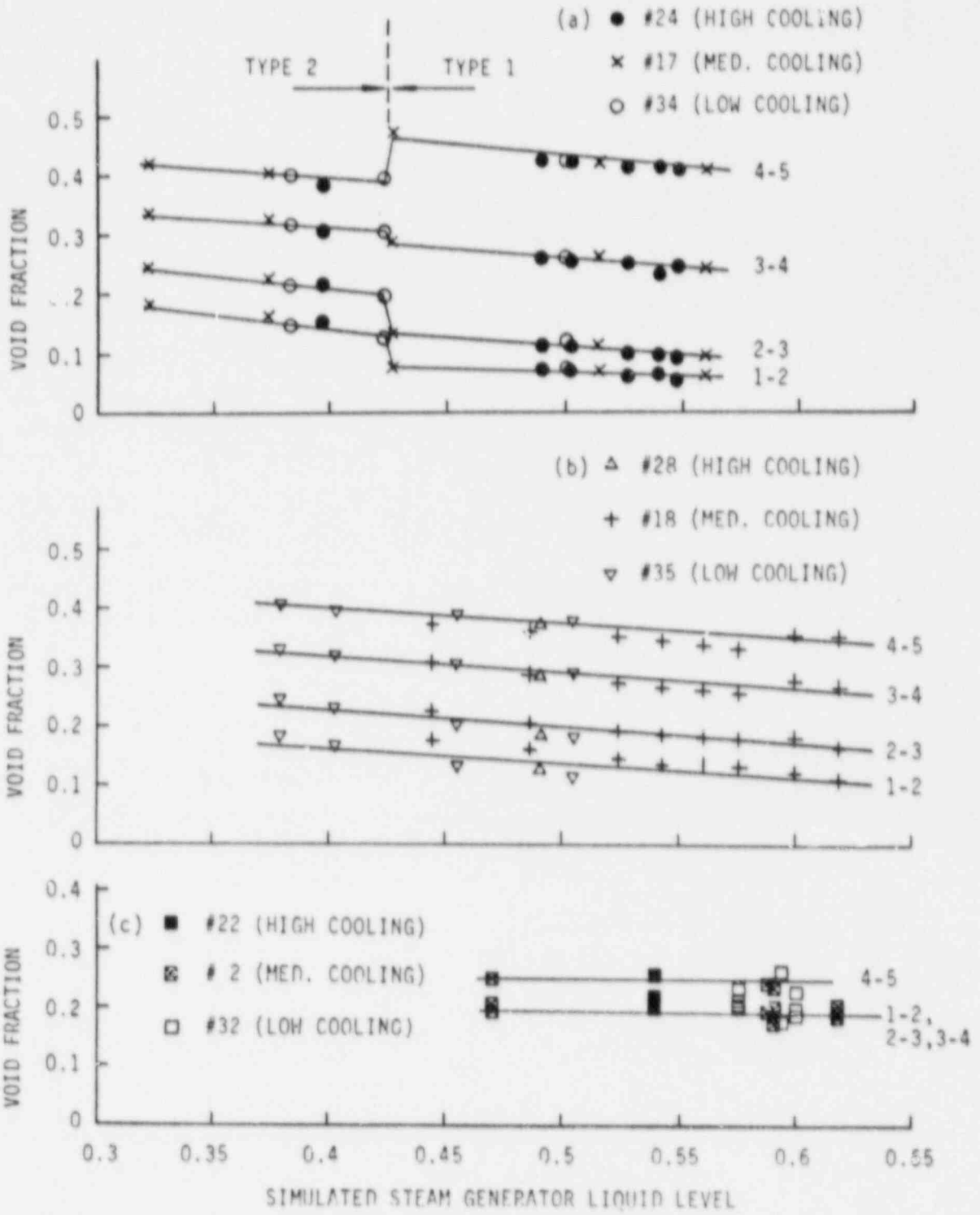

(a) Friction Control Valve Full-open, Power Input 2.2 KW
(b) Friction Control Valve 1/4-open, Power Input 2.2 KW
(c) Friction Control Valve Full-open, Power Input 1.3 KW

Fig. 12. Void Fraction of Each Riser Section of Hot-leg (Quasi-steady State)

only Type 2 oscillation is detected. This indicates that the system is more stabilized. When the power input is reduced (Fig. 12(c)), the void fraction inside the entire riser section decreases with low primary flow rate (Fig. 13(c)), and Type 2 oscillation is detected only.

b. Primary Loop Average Flow Rate

Figure 13 shows the change of the primary loop flow rate with the variation of the liquid level inside the simulated steam generator. For the case of the high power input with the friction control valve full-open (Fig. 13(a)), a sudden change of the flow rate is observed at certain liquid levels of the simulated steam generator by the same reason explained above, i.e., the change of the flow behavior from Type 1 to Type 2. Type 1 flow is characterized by the mild flashing with slug bubbles, and the flow rate is several times higher than the Type 2 flow in which the flow carry-over is maintained by the bubbly flow. When the opening of the friction control valve decreases (Fig. 13(b)) or at the low power input (Fig. 13(c)), Type 1 flow does not appear. Only Type 2 flow is observed. By comparing Fig. 13(a), (b), (c), it can be seen that the flow rates for Type 2 flow approximately merges into a single line. This indicates that the liquid level inside the simulated steam generator is one of the key parameters to determine the flow rate in the present experimental range. As the experiment continues longer, the liquid level inside the simulated steam generator slowly decreases further and the temperature of the fluid inside the loop increases gradually. This leads to higher void fraction two-phase flow inside the riser section with a higher natural circulation rate.

3. Measurement of Friction Resistance Coefficients

In order to analyze the natural circulation liquid flow interruption, it is necessary to obtain friction resistance coefficients of the test loop and the friction control valve at various openings. Similar to the approach of Hsu and Ishii [9], the system was operated under the forced circulation mode using the primary pump to measure the pressure drop. The differential pressure between the pump suction and discharge was measured by controlling the primary loop flow rates with two valves (fv and rv in Fig. 2; in this case the friction control valve fv can be used as one of the bypass valves). These

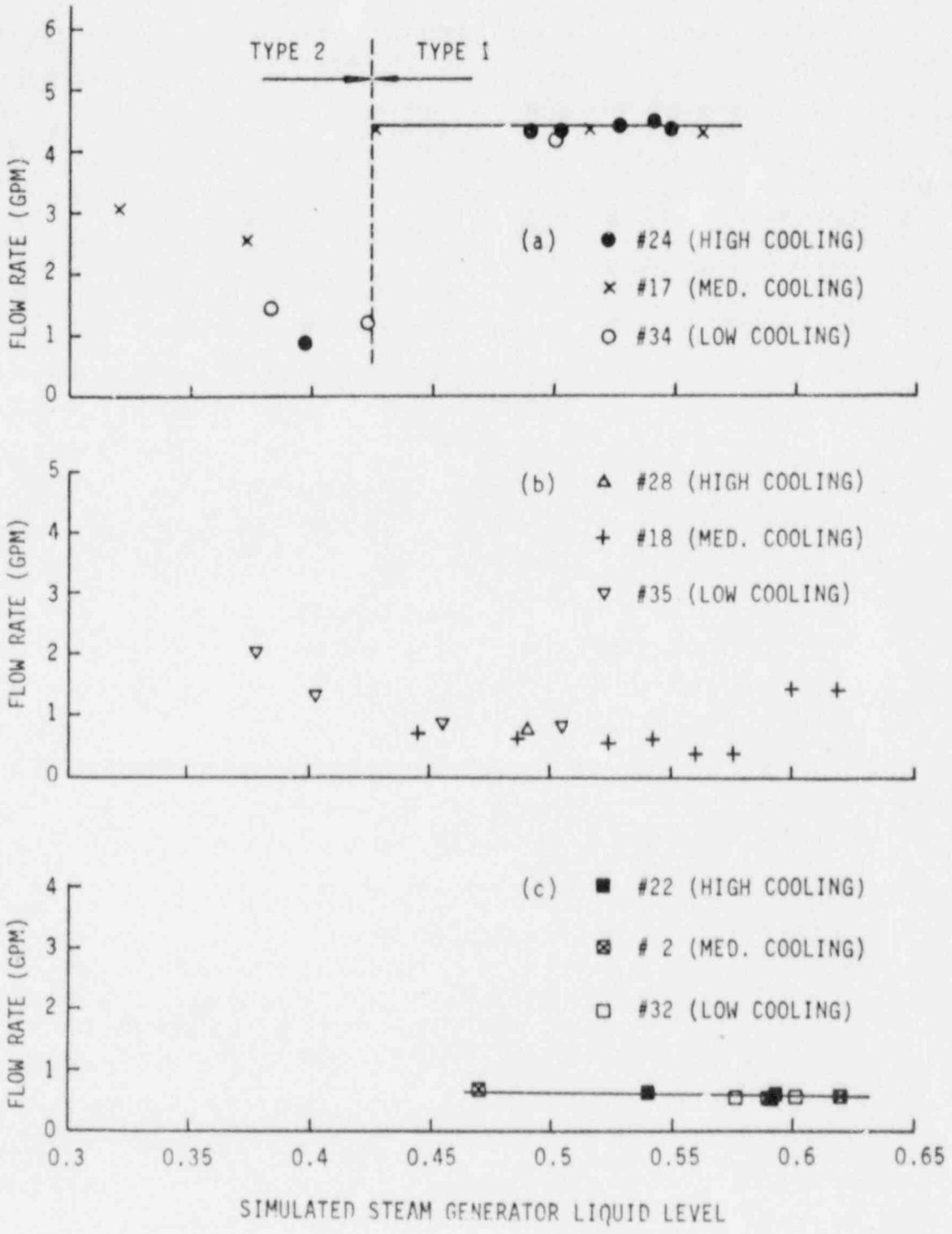

(a) Friction Control Valve Full-open, Power Input 2.2 KW
(b) Friction Control Valve 1/4-open, Power Input 2.2 KW
(c) Friction Control Valve Full-open, Power Input 1.3 KW

Fig. 13. Primary Loop Flow Rate (Quasi-steady State)

data were then used for the calculation of friction coefficient of the entire loop. For the measurement of the resistance coefficient of the friction control valve, the valve was separated out from the loop, and the pressure drop across the valve was measured using small calibration-loop with liquid (MERIAM No. D-8325, Indicating Fluid, Specific Gravity 1.75) manometer; water was used as the working fluid for this calibration purpose. Flow rates were measured by weighing the water collected in a container per unit time. All those measurements were listed in Tables A-2 and A-3 in Appendix.

It is noted that the friction control valve fully opened position corresponds to the simulation of the prototype system with the locked pump rotor resistance. Under the natural circulation conditions, the prototype pump rotor is considered to be locked in stationary position. For this case, the pump resistance is rather large compared with other hydraulic resistance. From Table A-2, the hot-leg equivalent K-value measured for the entire loop is about 37, which is close to the value of 45 in prototype system and the result of Hsu and Ishii [9].

VI. SUMMARY AND CONCLUSIONS

A Freon-113 flow visualization loop for simulating the hot-leg U-bend natural circulation flow has been constructed and hot-leg two-phase flow behavior was studied. Experimental results showed that the flow behavior depended significantly on the heat transfer and phase change effect, and strong non-equilibrium phenomena were observed. They are summarized as follows:

1. At the beginning of heating-up of the loop, the single-phase natural circulation is observed for a fairly long period. This is followed by cyclic flow behavior consisting of stable two-phase flow, sudden flashing, and suppression of boiling with flow termination. Those unsteady behaviors usually continue for three to six hours from the beginning of an experiment with a period of 4~15 minutes.

2. Unsteady flow is followed by a quasi-steady state flow. In this stage the flow becomes relatively stabilized, and no large-scale flow carry-over through the inverted U-bend associated with violent flashing was observed. However, several regular patterns of flow

oscillation are detected. These are the manometer oscillation with a period of 8-35 seconds and the density wave oscillation with a period of 2.5-4 minutes which is close to the residence time of a fluid around the loop. Along with a manometer oscillation, two different types of flow are observed. In the Type 1 oscillation, periodic mild flashing with a formation of short slug bubbles was observed with sizable amount of flow carry-over through the inverted U-bend. In Type 2 oscillation, continuous slow boiling along the riser section of the hot-leg in bubbly flow mode induced small flow carry-over through the inverted U-bend. Appearance of those types of oscillations depends strongly on the liquid level in the simulated steam generator, as well as the power input and friction control valve openings.

3. Significant variations of the void fraction were observed along the hot-leg. At the initial stage, the bottom section showed higher void fraction than the higher sections. This is due to the high-void churn-turbulent flow generated by 90° elbow at the bottom. However, near the top of the hot-leg, void fractions can become larger due to periodic flashing. At the later quasi-steady state mode, the void fraction increases along the hot-leg. This implies that, at the quasi-steady state, the boiling and evaporation in the hot-leg is more important than the entrance effect.

4. An average flow rate during the quasi-steady state mode strongly depends on the liquid level inside the simulated steam generator. Especially, Type 1 oscillation induces relatively larger flow rates due to the formation of slug bubbles by mild flashing.

Through the Freon-113 loop experiments, an understanding of the basic mechanism of the natural circulation and flow termination has been established. The power input, loop friction and the liquid level inside the simulated steam generator (thermal center) played key roles in determining natural circulation rate and flow behavior including flow oscillations inside the loop. The two-phase natural circulation with phase changes is shown to be much more unstable than the adiabatic two-phase flow. This is because the void distribution along the loop controls the natural circulation. For the case of the boiling and condensation loop, the amount of vapor in the loop is very sensitive to

the vapor generation and condensation rates which are strongly influenced by the hydrodynamic conditions. The coupling effects between the phase changes and hydrodynamic conditions tend to induce cyclic flow phenomena and flow oscillations.

ACKNOWLEDGMENTS

The authors would like to express their sincere appreciation to Drs. Novak Zuber and Richard Lee of NRC for valuable discussions and support on the subject. This work was performed under the auspices of the U.S. Nuclear Regulatory Commission. The experimental facility was constructed by Daniel J. Tucholke and W. C. Jeans in a very short time. The authors would like to thank their exceptional effort and excellent work.

REFERENCES

1. M. Ishii and I. Kataoka, "Similarity Analysis and Scaling Criteria for LWR's under Single-phase and Two-phase Natural Circulation," NUREG/CR-3267, ANL-83-32 (1983).

2. M. Ishii and I. Kataoka, "Scaling Laws for Thermal-hydraulic System under Single Phase and Two-phase Natural Circulation," Nucl. Eng. & Design, Vol. 81, pp. 411-425 (1984).

3. G. Kocamustafaogullari and M. Ishii, "Scaling Criteria for Two-phase Flow Natural and Forced Convection Loop and Their Application to Conceptual 2x4 Simulation Loop Design," NUREG/CR-3420, ANL-83-61 (1983).

4. G. Kocamustafaogullari and M. Ishii, "Scaling Criteria for Two-phase Flow Loop and Their Application to Conceptual 2x4 Simulation Loop Design," Nucl. Tech., Vol. 65, pp. 146-160 (1984).

5. H. R. Carter, "Mist Facility Status," Proc. 13th Water Reactor Safety Research Information Meeting, NUREG/CP-0072, Vol. 4, pp. 83-100 (1985).

6. G. Kocamustafaogullari and M. Ishii, "Reduced Pressure and Fluid to Fluid Scaling Laws for Two-phase Flow Loop," NUREG/CR-4584, ANL-86-19 (1986).

7. Z. Wang, M. Popp, M. Dimarzo, et al., "University of Maryland Test Facility Results," Proc. 13th Water Reactor Safety Research Information Meeting, NUREG/CP-0072, Vol. 4, pp. 47-82 (1985).

8. S. B. Kim and M. Ishii, "Flow Visualization Experiment on Hot-leg U-bend Two-phase Natural Circulation Phenomena," NUREG/CR-4621, ANL-86-27 (1986).

9. J.-T. Hsu and M. Ishii, "Experimental Study on Two-phase Natural Circulation and Flow Termination in a Loop," NUREG/CR-4682, ANL-86-32 (1986).

10. M. Ishii, S. Y. Lee, and S. Abou El-Seoud, "Results of Two-phase Natural Circulation in Hot-leg U-bend Simulation Experiments," Proc. 15th Water Reactor Safety Information Meeting, NUREG/CP-0091 (1988).

11. M. Ishii and O. Jones, Jr., "Derivation and Application of Scaling Criteria for Two-phase Flows," Two-phase Flows and Heat Transfer, Proc. NATO Advanced Study Institute, Istanbul, Turkey, Vol. 1, p. 163 (1976).

12. M. Ishii and N. Zuber, "Thermally Induced Flow Instabilities in Two-phase Mixtures," 4th Intl. Heat Trans. Conf., Paris, Paper B5.11 (1970).

13. N. Zuber, "Problems in Modelling of Small Break LOCA," in Heat Trans. in Nucl. Reactor Safety, S. G. Bankoff and N. H. Afgan, eds., p. 3, Hemisphere Pub. Corp. (1983).

14. N. Zuber and J. A. Findlay, "Average Volumetric Concentration in Two-phase Flow Systems," Trans. ASME, J. Heat Trans., Vol. 87, p. 453 (1965).

15. M. Ishii, "One-dimensional Drift-flux Model and Constitutive Equations for Relative Motion between Phases in Various Two-phase Flow Regimes," Argonne National Laboratory Report, ANL-77-47 (1977).

APPENDIX

EXPERIMENTAL DATA

Table A-1. Experimental Data on Temperature, Void Fraction and Flow Rate (Quasi-steady State)

Channel # / EXP. #	Temperature (mV, Type-T Thermocouple)							Void Fraction					Pressure Drop*	Flow Rate (GPM)	
	17	18	19	20	21	22	23	33	34	35	36	37	38	5	6
2	0.572	-	0.813	1.208	2.454	1.524	1.132	0.188	0.194	0.194	0.205	0.381	-0.001	-	0.582
	0.579	-	0.839	1.194	2.434	1.525	1.181	0.176	0.185	0.201	0.237	0.409	-0.001	-	0.512
	0.637	-	0.867	1.224	2.466	1.621	1.208	0.195	0.194	0.197	0.241	0.410	-0.007	-	0.526
	0.640	-	0.893	1.198	2.457	1.578	1.225	0.197	0.199	0.210	0.251	0.429	-0.006	-	0.629
17	0.812	-	1.374	1.378	2.419	1.588	1.698	0.162	0.228	0.325	0.403	0.627	-0.000	-	2.570
	0.811	-	1.374	1.335	2.411	1.592	1.704	0.180	0.247	0.338	0.420	0.679	0.001	-	3.084
	0.653	-	1.251	1.400	2.250	1.546	1.637	0.063	0.092	0.242	0.412	0.441	-0.001	-	4.280
	0.670	-	1.266	1.408	2.294	1.562	1.654	0.073	0.113	0.261	0.421	0.486	-0.003	-	4.352
	0.698	-	1.295	1.434	2.279	1.603	1.679	0.079	0.134	0.289	0.472	0.574	-0.006	-	4.360
18	0.709	-	1.320	1.145	2.346	1.406	1.609	0.112	0.166	0.268	0.356	0.382	-	-	1.463**
	0.712	-	1.320	1.151	2.350	1.410	1.604	0.123	0.178	0.275	0.356	0.400	-	-	1.457
	0.558	-	1.102	0.899	2.369	1.320	1.454	0.136	0.178	0.257	0.332	0.424	-0.166	-	0.402**
	0.566	-	1.114	0.883	2.370	1.329	1.464	0.138	0.182	0.263	0.338	0.440	-0.171	-	0.402**
	0.597	-	1.169	1.011	2.417	1.433	1.531	0.138	0.185	0.266	0.346	0.457	-0.119	-	0.630
	0.612	-	1.182	0.976	2.422	1.443	1.534	0.148	0.193	0.273	0.351	0.476	-0.112	-	0.563
	0.632	-	1.204	0.929	2.426	1.453	1.547	0.162	0.209	0.287	0.362	0.513	-0.110	-	0.638
	0.635	-	1.213	0.886	2.427	1.458	1.557	0.177	0.228	0.303	0.372	0.556	-0.108	-	0.718

*[psi].

**Average over 20 minutes.

Table A-1. Experimental Data on Temperature, Void Fraction and Flow Rate (Quasi-steady State) (CONT'D)

Channel # / EXP. #	Temperature (mV, Type-T Thermocouple)							Void Fraction					Pressure Drop*	Flow Rate (GPM)	
	17	18	19	20	21	22	23	33	34	35	36	37	38	5	6
22	0.619	-	0.771	1.257	2.454	1.637	1.185	0.178	0.178	0.171	0.263	0.406	-0.005	2.305	0.650
	0.622	-	0.798	1.241	2.492	1.627	1.201	0.200	0.210	0.218	0.258	0.461	-0.004	2.308	0.620
24	0.613	-	1.098	1.168	2.384	1.449	1.530	0.157	0.215	0.309	0.386	0.604	0.003	2.028	0.899
	0.608	-	1.127	1.392	2.286	1.532	1.589	0.076	0.115	0.255	0.426	0.497	-0.042	2.168	4.322
	0.660	-	1.127	1.454	2.274	1.544	1.587	0.069	0.098	0.236	0.419	0.460	-0.006	2.147	4.493
	0.672	-	1.149	1.453	2.288	1.564	1.617	0.074	0.116	0.261	0.432	0.510	-0.008	2.151	4.339
	0.711	-	1.202	1.524	2.248	1.585	1.630	0.059	0.093	0.249	0.409	0.452	-0.009	2.179	4.333
	0.710	-	1.202	1.518	2.254	1.582	1.641	0.062	0.099	0.258	0.417	0.473	-0.009	2.178	4.423
28	0.628	-	1.089	1.143	2.356	1.448	1.521	0.130	0.187	0.287	0.374	0.509	-0.131	2.120	0.774
32	0.598	-	0.801	1.075	2.486	1.590	1.105	0.204	0.201	0.190	0.226	0.400	0.001	-	0.579
	0.602	-	0.826	1.013	2.466	1.580	1.135	0.214	0.208	0.201	0.234	0.424	0.001	-	0.519
34	0.644	-	1.253	1.374	2.306	1.528	1.652	0.078	0.121	0.262	0.428	0.500	0.001	-	4.218
	0.670	-	1.293	1.327	2.381	1.541	1.637	0.127	0.198	0.308	0.398	0.577	-0.001	-	1.203
	0.670	-	1.290	1.271	2.388	1.527	1.636	0.150	0.219	0.320	0.404	0.617	-0.001	-	1.428
35	0.652	-	1.263	1.223	2.379	1.514	1.604	0.112	0.182	0.291	0.382	0.495	-0.158	-	0.895
	0.670	-	1.279	1.189	2.384	1.522	1.611	0.140	0.205	0.309	0.394	0.546	-0.151	-	0.905
	0.685	-	1.291	1.171	2.403	1.533	1.632	0.170	0.232	0.325	0.402	0.597	-0.158	-	1.369
	0.694	-	1.297	1.187	2.408	1.547	1.658	0.186	0.248	0.335	0.407	0.622	-0.185	-	2.004

*[psi].

Table A-2. Resistance Coefficients for the Test Loop*

Liquid (Freon-113) Velocity (cm/s)	ΔP (N/m^2)	K Value $K = \Delta P/(\frac{1}{2}\rho_f u_f^2)$
20.6	997	31.12
30.3	2572	37.20
32.2	2916	37.28
38.5	4181	37.47
40.7	4726	37.75
41.4	4915	37.90
45.9	5912	37.17
49.1	6915	38.02
51.7	7635	37.87
53.4	8181	37.95
58.7	9904	38.07
62.3	11157	38.07
62.4	11049	37.56
68.4	13244	37.49
74.5	15588	37.23
80.2	17924	36.93
80.2	17688	36.45
85.0	19978	36.66
88.5	21661	36.61

*Based on the hot-leg I.D. (5 cm).

Table A-3. Resistance Coefficients for 2" Full-port Ball Valve*

Friction Control Valve Opening	Liquid (Water) Velocity (cm/s)	ΔP (N/m^2)	K Value $K = \Delta P/(\frac{1}{2}\rho_f u_f^2)$
Full-open	54.9	18.67	0.124
	64.4	28.01	0.135
3/4-open	18.0	56.01	3.46
	36.7	214.7	3.19
	46.7	429.4	3.94
	53.1	560.1	3.97
	57.3	644.1	3.92
	62.6	765.5	3.91
	63.7	784.1	3.86
	63.8	793.5	3.90
1/2-open	5.22	37.34	27.4
	18.1	560.1	34.2
	31.5	1792	36.1
	44.4	3547	36.0
	49.1	4387	36.4
3/8-open	2.63	46.68	135.0
	6.57	354.7	164.3
	11.3	1036	162.3
	14.9	1830	164.9
	18.3	2763	165.0
	22.4	4154	165.6
1/4-open	2.02	438.7	2150
	3.21	1064	2065
	4.95	2511	2050
	6.05	3762	2056
	6.86	4873	2071
3/16-open	0.612	1624	86719
	0.883	3295	84521
	1.09	4976	83764

*Calibrated with water.

NRC FORM 335 (2 84) NRCM 1102 3201, 3202

U.S. NUCLEAR REGULATORY COMMISSION

BIBLIOGRAPHIC DATA SHEET

SEE INSTRUCTIONS ON THE REVERSE

1 REPORT NUMBER (Assigned by TIDC add Vol No. if any)

NUREG/CR-5082
ANL-88-1

2 TITLE AND SUBTITLE

SIMULATION EXPERIMENTS ON TWO-PHASE NATURAL CIRCULATION IN A FREON-113 FLOW VISUALIZATION LOOP

3 LEAVE BLANK

4 DATE REPORT COMPLETED

MONTH: December YEAR: 1987

5 AUTHOR(S)

Sang Yong Lee and Mamoru Ishii

6 DATE REPORT ISSUED

MONTH: January YEAR: 1988

7 PERFORMING ORGANIZATION NAME AND MAILING ADDRESS (Include Zip Code)

Reactor Analysis and Safety Division
Argonne National Laboratory
9700 S. Cass Avenue
Argonne, Illinois 60439

8 PROJECT/TASK/WORK UNIT NUMBER

9 FIN OR GRANT NUMBER

A2026

10 SPONSORING ORGANIZATION NAME AND MAILING ADDRESS (Include Zip Code)

Division of Accident Evaluation
Office of Nuclear Regulatory Research
U.S. Nuclear Regulatory Commission
Washington, D.C. 20555

11a TYPE OF REPORT

Technical

b PERIOD COVERED (Inclusive dates)

Feb. 1987 - Dec. 1987

12 SUPPLEMENTARY NOTES

13 ABSTRACT (200 words or less)

In order to study the two-phase natural circulation and flow termination during a small break loss of coolant accident in LWR, simulation experiments have been performed using a Freon-113 flow visualization loop. The main focus of the present experiment was placed on the two-phase flow behavior in the hot-leg U-bend typical of B&W LWR systems. The loop was built based on the two-phase flow scaling criteria developed under this program to find out the effect of fluid properties, phase changes and coupling between hydrodynamic and heat transfer phenomena. Significantly different flow behaviors have been observed due to the non-equilibrium phase change phenomena such as the flashing and condensation in the Freon loop in comparison with the previous adiabatic experiment. The phenomena created much more unstable hydrodynamic conditions which lead to cyclic or oscillatory flow behaviors. Also, the void distribution and primary loop flow rate were measured in detail in addition to the important key parameters, such as the power input, loop friction and the liquid level inside the simulated steam generator.

14 DOCUMENT ANALYSIS - a KEYWORDS/DESCRIPTORS

Two-phase Flow
Natural Circulation
Hot-leg U-bend
Flashing
Scaling Criteria
Flow Oscillation
Void Fraction
Freon-113 Loop

b IDENTIFIERS/OPEN ENDED TERMS

15 AVAILABILITY STATEMENT

Unlimited

16 SECURITY CLASSIFICATION

(This page) Unclassified

(This report) Unclassified

17 NUMBER OF PAGES

18 PRICE

Distribution for NUREG/CR-5082 (ANL-88-1)

Internal:

C. E. Till
J. F. Marchaterre
A. J. Goldman
L. W. Deitrich
D. Rose
D. H. Cho
B. W. Spencer
W. T. Sha
Y. W. Shin
J. Sienicki
D. W. Condiff
S. Y. Lee (6)
M. Tan
N. T. Obot
Y. S. Cha
A. C. Raptis
M. Ishii (22)
ANL Patent Dept.
ANL Contract File
ANL Libraries
TIS Files (3)

External:

USNRC Washington, for distribution per R2 and R4 (325)
DOE-TIC (2)
Manager, Chicago Operations Office
Reactor Analysis and Safety Division Review Committee:
W. B. Behnke, Jr., Commonwealth Edison Co., Chicago, Ill. 60690
M. J. Ohanian, Univ. of Florida, Gainesville, Fla. 32611
R. L. Seale, Univ. of Arizona, Tucson, Ariz. 85721
J. S. Armijo, General Electric Company, San Jose, Calif. 95153-5354
T. J. Hirons, Los Alamos National Laboratory, Los Alamos, N. Mex. 87545
N. E. Todreas, Mass. Inst. of Technology, Cambridge, Mass. 02139
A. E. Dukler, Univ. of Houston, Tex. 77004
O. C. Jones, Rensselaer Polytechnic Inst., Troy, N. Y. 12181
G. Kocamustafaogullari, Univ. of Wisconsin-Milwaukee, Milwaukee, Wis. 53201
K. A. Williams, Science Applications International, Albuquerque, N. Mex. 87102